Seismic safety of valuable non-structural elements in RC buildings: Floor Response Spectrum approaches

SEISMIC SAFETY OF VALUABLE NON-STRUCTURAL ELEMENTS IN RC BUILDINGS: FLOOR RESPONSE SPECTRUM APPROACHES

Luisa Berto[(1)]* – Marco Bovo[(2)] – Irene Rocca[(1)]

Anna Saetta[(1)] - Marco Savoia[(3)]

[(1)]DCP – University IUAV of Venice, Campus Terese, Dorsoduro 2206, 30123 Venezia - Italy

[(2)]DISTAL - University of Bologna, Viale Giuseppe Fanin, 44, 40127 Bologna - Italy

[(3)] DICAM - University of Bologna Viale Risorgimento, 2 - 40136, Bologna - Italy

** corresponding author: tel +39 041 2571311 - +39 049 8789913 e-mail: lberto@iuav.it*

Abstract

The seismic performances of non-structural (NS) components belonging to the category of "valuable elements", i.e. elements characterized by high value in terms of economic, cultural or strategic purposes, represent nowadays a crucial aspect in seismic safety design and assessment of new and existing buildings. Actually, most valuable NS elements are simply-supported objects, which can be classified as acceleration-sensitive NS elements. Frequently, these elements can be considered dynamically uncoupled from the primary structure to which they are connected, thereby justifying the Floor Response Spectrum methods usually adopted in literature and by most of building codes. This paper presents an extensive parametric study of floor response spectra obtained by linear and nonlinear numerical modeling of RC structures. Two sets of 30 horizontal ground motion scaled acceleration records are generated according to the Ultimate Limit State (ULS) and the Damage Limitation State (DLS) spectra adopted for building design. The numerical floor response spectra and those proposed by

codes and international standards are critically compared, and the Peak Floor Acceleration (*PFA*) and the Peak Floor Velocity (*PFV*) profiles along the building height are discussed. Finally, a simplified method based on the "stability charts" is developed to assess the seismic safety of free standing NS elements located at the upper floors of the host buildings.

Keywords: non-structural elements; floor response spectra; valuable elements; seismic assessment; building codes; seismic demand

1 Introduction

In recent years, the harmonization of seismic performance levels between structural and non-structural (NS) elements has become crucial. The experience derived from many past earthquakes has shown that failure of NS elements can affect life safety causing injuries or deaths, hampering safe evacuation of occupants and rescue operations. Moreover, non-structural damage often limits the functionality of critical facilities (such as hospitals, fire stations) even after frequent and less intense earthquakes [1], [2], [3], [4]. Finally, for many buildings NS elements, including building contents, constitute a considerable amount (70−80 percent) of the total construction value [5]. Consequently, in many past earthquakes losses derived from the damage of NS elements exceeded losses related to structural damage. This issue becomes even more crucial if we consider that significant non-structural damage can also occur at low seismic intensity levels, for which structural elements are expected to remain in their elastic domain.

These observations make clear that the seismic performances of NS elements have importance comparable with that of structural components. Nevertheless, in comparison with structural elements, much less information on seismic design and on the seismic assessment of NS elements, especially in existing buildings, is available. The research work in this area is sparse, and the current Standards and Guidelines have been mostly developed on the basis of empirical approaches, related to past experiences and engineering expertise [1], [6].

According to Filiatrault and Sullivan [1], the NS elements are classified into three macro groups: architectural components, mechanical and electrical components, and building contents. Specific architectural components include built-in NS components constituting the building itself, like partition walls, parapets, chimneys, suspended ceilings. Mechanical and electrical components include HVAC equipment, engines, turbines, generators, communication equipment, computers, and batteries. Lastly, building contents include all the NS components belonging to “the occupants” of the building, like filing cabinets, bookshelves

and all furniture inside the building.

Among the building contents, a particular category is represented by the "valuable NS elements", that are characterized by high value. Actually, the category of valuable NS elements comprehends elements that, due to their economic, cultural or strategic importance, cannot be damaged in the case of seismic events (e.g., medical devices, plants, data servers, artistic assets - both exposed or stored) and, therefore, have to be protected.

In many cases, the valuable elements are simply-supported (i.e. free standing) objects, or at least weakly connected to the structure, and can be classified in the category of the so-called "acceleration-sensitive" NS elements. When these NS elements are located on the upper floors of the host building, particular attention must be paid to the evaluation of the seismic demand. To this aim, the most common methods are based on the floor response spectra, which allow performing an uncoupled analyses of the NS element and the host building, e.g. [1], [7]. Floor Response Spectrum (FRS) method, which actually neglects the dynamic structure-object interaction, can be satisfactorily adopted for NS elements with a mass at least one thousand smaller than that of the structure, even when their natural frequencies are tuned [8], [9], [10].

Within the FRS framework, the present paper initially focuses on the characterization of the seismic input acting at the base of an NS element located in the upper floors of buildings. Then, an extensive parametric study on floor response spectra obtained by linear and nonlinear time-history analyses on numerical models of 2D Reinforced Concrete (RC) structures, is performed. Two different building typologies, i.e. Moment Resisting Frames (*MRF*) and slender Cantilever Wall (*CW*) systems, with equal first mode vibration period, are considered, in order to investigate the effect on the FRS of different mode shapes and of higher modes.

Nowadays, most of the FRS approaches proposed by codes and international standards, e.g. [11], [12], [13], depend only on the fundamental vibration mode along the relevant direction

without considering the effects of different mode shapes. This aspect, in the authors' opinion, may represent a critical issue and should be dealt with in future improvements of FRS proposal. In particular, the cases of irregular buildings (in plan and/or elevation) and torsion-deformable structures need to be deeply investigated.

In the present study, two different sets of 30 horizontal ground motion scaled records, respectively obtained imposing the compatibility between the spectrum at Ultimate Limit State (ULS) and at Damage Limitation State (DLS) adopted for building design are considered. The large number of input motions considered has allowed to underline some significant aspects and to obtain practical indications on floor amplification versus floor height, related to different earthquake Intensity Measures (*PGA*, *PGV*, *PFA*, *PFV)* and different RC building typologies. For the first set of ground motions, compatible with the ULS spectrum, the behavior of the buildings is investigated also in a wide nonlinear range. By means of the second set of 30 ground motion records, which is compatible with the prescribed target spectrum at DLS, the structural behavior is investigated by assuming the absence of significant damage in the structural elements.

Finally, in this paper a practical procedure for free standing NS elements located in the RC building is proposed, extending the practical tools for the large-scale seismic vulnerability assessment of elements located at the ground floor (i.e. *"stability charts"*) proposed in [14], to the case of objects located at the upper floors of host buildings. The charts allow assessing the stability conditions of an NS element, given its geometry, its placement inside the building, and the seismicity of the site. The charts can be used also as predictive tools, for instance to identify the maximum floor level at which the object can be safely located i.e. avoiding overturning or rocking occurrence.

2 Floor Response Spectrum (FRS) approaches

One of the main aspects to be considered in dealing with design criteria for NS elements is the

forces distribution over the height of the host building. As previously stated, the Floor Response Spectrum (FRS) approach represents one of the most common methods to evaluate the filtering effect of the host building and estimate the horizontal acceleration at each floor level of the building itself. When dealing with acceleration-sensitive NS elements, these accelerations are the base for calculating the seismic design forces acting on the NS component.

Actually, the primary structure, with its dynamic response, modifies the seismic signal at ground level, altering both its frequency content and its amplitude. It is evident that an accurate evaluation of the dynamic response of an NS element located within a structure subjected to a seismic action would require sophisticated numerical analyses, considering the coupled motion of the host structure and NS element, i.e. the so-called “direct analysis” approach.

If the mass of the NS element is much smaller than that of the main structure, the motion can be considered decoupled, and the so-called "cascading approach" can be profitably adopted, in which structure and secondary element are analyzed separately, e.g. [15], [1]. The value of the ratio of the NS mass to the mass of the primary structure for which interaction effects can be neglected is a highly debated issue, see for instance [16]: some authors state that the mass of the NS must be smaller than the mass of the primary structure by a factor of more than one hundred [17], [18]; other studies, as cited in [9], [16] and [19], state that this interaction may be important also when the ratio ranges in the interval 1/100 - 1/1000. In any case, the cascade approach, neglecting the dynamic interaction between the NS element and its supporting structure, generally gives too conservative results, [10], [20].

In this context, one of the most used cascading approaches is the method based on the formulation of the floor response spectra. These spectra can be obtained following two different approaches, characterized by different accuracy levels:

- *direct generation via time history analyses*. The floor response spectra are directly

derived starting from floor acceleration signals obtained with time-history analyses of the structure, subject to a series of spectrum-compatible accelerograms at ground level. Numerical analyses can be performed with reference to elastic or inelastic models of the building, e.g. [16], [21];

- *spectrum-to-spectrum formulations.* The floor response spectra are directly estimated via predictive equations depending on ground floor spectra and some dynamic properties of the primary structure and of the NS element (e.g. mode vibration periods, damping ratio). Different formulations can be found in literature and in building codes, which are generally design-oriented and developed on the basis of empirical, analytical and/or numerical studies. (e.g. [8], [10] - [13], [17], [22], [23]). Note that building irregularities are rarely accounted for in this approach, as the building response is primarily related to translational response.

In the following, a brief overview of the most common spectrum-to-spectrum formulations adopted in European and International Standards is presented. These formulations can be subdivided into two main categories, respectively labeled as "practical spectrum-to-spectrum-approaches", due to their practice-oriented formulations, and "modal superposition spectrum-to-spectrum-approaches". The first are based on simplified equations and consider the filtering effect of the primary structure in an approximate way, at most through its fundamental period, while the second ones take into account the main dynamic features of the structure, e.g. frequencies, modal shapes and modal participation coefficients of the relevant vibration modes.

2.1 Practical spectrum-to-spectrum approaches

2.1.1 EC8 proposal

According to Eurocode 8 [11], the acceleration S_a to which an NS element with period T_a located at the height z, is exposed, considering also the effect of the behaviour factor q_a of the

NS element is evaluated as:

$$S_a(T_a, z) = \frac{PGA}{q_a} \cdot \left[\frac{3 \cdot (1 + z/h_b)}{1 + (1 - T_a/T_1)^2} - 0.5 \right] \geq \frac{PGA}{q_a} \quad (1)$$

where T_1 is the fundamental period of the structure in the direction of the seismic action, h_b the total building height measured from the foundation level, q_a is assumed equal to 1.0 or 2.0 depending on the type of NS element and $PGA = S\, a_g$ is the peak ground acceleration (given by the product of the soil factor S and the design ground acceleration on type A ground, a_g), for the considered limit state of the structure, ground type and topography condition.

A key point is that the EC8 approach only considers the amplification associated with the fundamental vibration mode of the primary structure in the relevant direction, whereas the FRS can be significantly affected by higher modes of vibration, especially in the case of tall buildings, e.g. [15], [24]. Although the simplicity and wide use of this approach, indeed, it is by now acknowledged that EC8 approach may underestimate the acceleration demand on NS elements for a wide range of periods, especially when they are close to those of higher modes of the primary structure. On the other hand, the cutoff lower limit imposed by EC8 formulation (i.e. the *PGA* value) leads to an amplification of the seismic signal overly conservative for long periods T_a, for which the filtering effect of the structure becomes negligible according to this formulation.

At the roof level, EC8 proposal predicts a peak elastic acceleration for the NS element with a fundamental vibration period equal to that of the structure, i.e. for $T_a = T_1$, about 5.5 times the peak ground acceleration (*PGA*) when the NS element is designed to remain elastic ($q_a = 1.0$).

It is worth noting that the EC8 approach, eq. (1), does not explicitly consider the effect of non linearity of the primary structure, but it includes this effect in an approximate way, i.e. without distinguishing the level of attained ductility of the structure itself, e.g. Vukobratovik

and Fajfar [17] and Petrone et al. [21]. Moreover, this approach takes the non linearity of the NS element into account just through the NS behavior factor q_a.

2.1.2 ASCE 7-10 formulation

The seismic design requirements for NS elements in the United States are given by ASCE 7-10 [12], in terms of design force F_p for acceleration-sensitive NS elements. An interesting evaluation of ASCE 7-10 equations, using FRS data obtained from a series of instrumented buildings, can be found in Anajafi and Medina [6].

According to [6], the acceleration S_a to which an elastic NS element with period T_a is subjected can be expressed as:

$$S_a(T_a, z) = PGA \cdot \frac{a_p[1 + 2(z/h_b)]}{R_p} \tag{2}$$

where R_p is the NS response modification factor, that is a reduction factor between 1.0 and 12.0 depending on which of the 56 different types of NS elements is considered (see Table 13.5-1 of ASCE 7-10 [12]). The term $[1 + 2(z/h_b)]$ represents an estimation of the ratio between the Peak Floor Acceleration and the Peak Ground Acceleration (*PFA*/*PGA)*. This term approximates the mean plus one standard deviation of the recorded floor accelerations for a series of instrumented buildings subject to peak ground accelerations of at least 0.10g [2]. The parameter a_p is the NS amplification factor, depending on the period T_a of the NS element itself. This parameter is equal to 1.0 for rigid NS elements ($T_a \leq$ 0.06s) and 2.5 for flexible elements (T_a>0.06s).

It is worth noting that, according to eq. (2), the predicted maximum acceleration S_a acting on a flexible NS element is up to 7.5 times *PGA* when $R_p = 1$. However, the code does impose a limit on the maximum design force, that could be interpreted as a limitation to the peak acceleration of the NS element, of 4.0 times *PGA* [6]. Finally, similarly to EC8 code, the ASCE 7-10 proposal does not explicitly take into account the reduction of the FRS due to the

nonlinear behavior of the primary structure. However, the adoption of low a_p values could include this effect even if in an approximate way, see Petrone et al. [21] and Anajafi and Medina [6].

2.1.3 NZS 1170.5 formulation

The NZS 1170.5 Standard, [13] defines the seismic action on NS elements according to a force formulation, which can be written in terms of the floor spectrum as follows:

$$S_a(T_a, z) = PGA\ C_{Hi}(z) C_i(T_a) C_{ph}\ R_p \leq 3.6g \tag{3}$$

where $C_{Hi}(z)$ and $C_i(T_a)$ are, respectively, the floor height coefficient relative to *i-th* floor and the coefficient that defines the spectral shape relative to the NS element at *i-th* floor (Figure 1); R_p is the component risk factor, function of the risk associated with a possible collapse of the element; C_{ph} is the horizontal response factor of the NS component, function of the component ductility and *g* the gravity acceleration.

It is worth noting that the NZS proposal predicts a peak acceleration on NS elements at the roof level equal to 6.0 times *PGA* when $C_{ph} = 1$ and $R_p = 1$, but, unlike Eurocode 8, this value does not depend on the period of the host structure.

2.1.4 MIT19 simplified formulation for MRF

The Commentary of Italian Standard [25] provides a simplified FRS formulation for *MRF* buildings. In this case, the spectral acceleration $S_a(T_a, z)$, considering also in this formulation the q_a factor, is expressed by:

$$S_a(T_a, z)$$

$$= \frac{1}{q_a} \begin{cases} PGA\left(1+\frac{z}{h_b}\right)\left[\frac{a_p}{1+(a_p-1)\left(1-{}^{T_a}/_{aT_1}\right)^2}\right] \geq PGA \quad for\ T_a < aT_1 \\ PGA\left(1+\frac{z}{h_b}\right) a_p \qquad\qquad for\ aT_1 \leq T_a < bT_1 \\ PGA\left(1+\frac{z}{h_b}\right)\left[\frac{a_p}{1+(a_p-1)\left(1-{}^{T_a}/_{bT_1}\right)^2}\right] \geq PGA \quad for\ T_a \geq bT_1 \end{cases} \tag{4}$$

where a, b and a_p are parameters defined according to the fundamental period of the primary structure (Table 1). These parameters have been calibrated taking into account both the elongation of the fundamental period due to system non linearity, and the contribution of the higher modes. This proposal (in the following referred to as MIT19-MRF) derives from the work of Petrone et al. [24] and from some indications of Fathali and Lizunda [26]. The resulting FRS gives, in general, conservative values for a wide range of periods, in particular for NS elements with a fundamental period close to the one of the primary structure.

2.2 Modal superposition spectrum-to-spectrum approaches

2.2.1 MIT19 general formulation

The general proposal presented in the Commentary of Italian Standards [25] (in the following referred to as MIT19-Nmodes) is based on a modal superposition approach. It can be applied to any type of buildings.

According to this proposal, the acceleration acting on the NS element located at the *j-th* floor, due to the effect of the *i-th* vibration mode of the structure with period T_i, is given by:

$$S_{a,ij}(T_a, \xi_a) = \Gamma_i \varphi_{ij} S_e(T_i)\, R\left(\frac{T_a}{T_i}; \xi_a\right) = PFA_{ij} R\left(\frac{T_a}{T_i}; \xi_a\right) \tag{5}$$

where $S_e(T_i)$ is the spectral ground acceleration of the *i-th* mode, possibly reduced through the behavior factor q of the construction to take the nonlinear behavior of the primary

structure into account; Γ_i is the modal participation factor and φ_{ij} is the *j-th* component of the *i-th* modal shape normalized to the maximum value; *R* is the amplification factor of the PFA_{ij}, which depends on the damping coefficient ξ_a of the NS element and on T_a/T_i ratio according to the relationship:

$$R = \left[\left(2\xi_a \frac{T_a}{T_i}\right)^2 + \left(1 - \frac{T_a}{T_i}\right)^2\right]^{-\beta} \tag{6}$$

The amplification factor *R* considers the coupling between the *i-th* vibration mode of the structure and the fundamental mode of the NS element through the coefficient β (variable between 0.4 and 0.5). Finally, the actual acceleration on the NS component is obtained by properly combining the responses relative to the different modes, eq. (5), e.g. through SRSS rule.

2.2.2 MIT19 simplified formulation

The Commentary of Italian Standard provides also a simplified multi-modal formulation (in the following referred to as MIT19-Simp-Nmodes) based on recent research, e.g. [20], [22]. According to this formulation, the acceleration acting on the NS element located at the height *z*, due to the effect of the *i-th* vibration mode of the structure with period T_i and viscous damping ratio ξ_i (expressed as a percentage), is given by:

$$S_{a,i}(T_a, \xi_a, z) = \begin{cases} \dfrac{11\xi_i^{-0.5}\eta(\xi_a)PFA_i(z)}{1 + [11\xi_i^{-0.5}\eta(\xi_a) - 1]\left(1 - {}^{T_a}/_{aT_i}\right)^{1.6}} & for\ T_a < aT_i \\ 11\xi_i^{-0.5}\eta(\xi_a)PFA_i(z) & for\ aT_\mathrm{i} \le T_a < bT_i \\ \dfrac{11\xi_i^{-0.5}\eta(\xi_a)PFA_i(z)}{1 + [11\xi_i^{-0.5}\eta(\xi_a) - 1]\left({}^{T_a}/_{bT_i} - 1\right)^{1.2}} & for\ T_a \ge bT_i \end{cases} \tag{7}$$

where a = 0.8 and b = 1.1 are parameters defining the range of periods of maximum amplification of the spectrum, $\eta(\xi_a) = \sqrt{10/(5 + \xi_a)}$ is the damping correction factor for the NS element with ξ_a expressed as a percentage, while the contribution of the *i*-th mode to the

peak floor acceleration at the height z, $PFA_i(z)$, is given by:

$$PFA_i(z) = S_e(T_i, \xi_i)|\Gamma_i \varphi_i(z)|\sqrt{1 + 0.0004\xi_i^2} \tag{8}$$

with $\varphi_i(z)$ the i-th modal shape of the building at the height z and Γ_i the modal participation factor.

Also in this case, the actual acceleration acting on the NS component is finally obtained by properly combining the contributions due to the different modes, eq. (7), through SRSS rule:

$$S_a(T_a, \xi_a, z) = \sqrt{\sum \left[S_{a,i}(T_a, \xi_a, z)\right]^2} \geq S_e(T_a, \xi_a) \quad for\ T_a > T_1 \tag{9}$$

In any case, the acceleration acting on the NS element with $T_a > T_1$ must always be greater than the spectral ground acceleration $S_e(T_a, \xi_a)$, evaluated in correspondence of the period T_a of the NS element. The peak floor acceleration at the height z, $PFA(z)$, is therefore given by:

$$PFA(z) = \sqrt{\sum [PFA_i(z)]^2} = \sqrt{\sum \left[S_e(T_i, \xi_i)|\Gamma_i \varphi_i(z)|\sqrt{1 + 0.0004\xi_i^2}\right]^2} \tag{10}$$

The non linearity of the structure could be included in this formulation by increasing both the period T_i and the viscous damping ξ_i, as a function of the ductility demand (refer to [20] for further details).

2.3 Discussion and remarks

Among the practical spectrum-to-spectrum approach, the formulations of EC8, ASCE 7-10 and NZS 1170.5 are applicable to all the building typologies, while the MIT19-MRF is applicable only to *MRF* systems. These formulations consider the building response at most through its fundamental period and do not explicitly account for the non linearity of the host building.

The modal superposition spectrum-to-spectrum formulations suggested in the Italian Standards are applicable to any buildings typology. They consider the modal response of the

building also for the higher modes and include the nonlinear behavior of the host structure in an explicit way: for MIT19-Nmodes through an elongation of the fundamental period and the introduction of a behavior factor q of the construction and for MIT19-Simp-Nmodes by adopting overdamped spectrum and fundamental period elongation.

It is worth noting that in the above-described formulations there is no explicit mention of the material of construction, but in the authors' opinion the MIT19-MRF – in particular the calibration of the a_p, a and b parameters – should be intended for reinforced concrete MRF, as treated in the study of Petrone [24]. Moreover, the MIT19-Simp-Nmodes has been introduced in the new draft of Eurocode 8-Part 3 specifically for masonry buildings.

3 Seismic vulnerability assessment of free standing NS elements

The seismic vulnerability of free standing NS elements can be effectively assessed by using rigid block models that consider the limit equilibrium of the element - or of its parts - with reference to the possible different rigid body motions (i.e. rocking, overturning, sliding). In the past decades, rigid block modeling has been extensively investigated, starting from the pioneering work of Housner [27]. The most common methods can be generally subdivided into simplified and advanced approaches. The first ones are based on operational criteria that refer to the main inertial properties of the body and to some seismic intensity measures, (*PGA*, *PGV*, spectral displacement S_d, etc.), e.g. Ishiyama [28], [29] Lam and Gad [30]. Instead, the advanced methods are usually based on non-linear dynamic analyses, requiring the numerical integration of the equations of motion, see [31], [32], [33], [34], [35] among many others, and are in many cases used to provide fragility curve for estimating the probability of overturning, e.g. [36],[37],[38].

As far as the simplified methods are concerned, an effective tool is represented by the "stability charts", which can be created adopting different approaches to evaluate the safety of NS elements, e.g. [14]. These charts allow to assess the seismic vulnerability of free standing

objects in terms of rocking and overturning motions (assuming that the friction coefficient is large enough to avoid sliding), as a function of the geometrical characteristics of NS element as well as of the site in terms of seismic action (e.g. *PGA*, *PGV*, spectral acceleration, spectral velocity).

In the present paper, the stability charts are created adopting the Ishiyama proposal [28], [29], which involves, for the overturning assessment, two different criteria based on acceleration and velocity, respectively.

The acceleration criterion states that the minimum acceleration value that can activate the overturning motion is $a_{g,c}= B/H,$ which corresponds to the rocking condition itself. In this expression, B represents the minimum distance between the projection of the center of mass of the body and the base edge around which the oscillation occurs, and H is the height of the center of mass.

Concerning the velocity criterion, the minimum horizontal velocity value necessary to trigger overturning is given by the critical velocity v_c that, in the case of a rectangular and slender block (with $H > 3B$), can be expressed as:

$$v_c = 0.4\sqrt{\frac{4}{3}\frac{gB^2}{H}} \tag{11}$$

In the case of slender objects with generic shape, eq. (11) is still valid by introducing the concept of equivalent height, see [39].

In the present work, the seismic vulnerability assessment of the NS element is carried out by comparing the capacity, evaluated according to the Ishiyama proposal, with the corresponding demand, as follows:

- stability: $a_{max} < a_{g,c}$,
- rocking: $a_{max} \geq a_{g,c}$ and $v_{max} < v_c$ (12)
- overturning: $a_{max} \geq a_{g,c}$ and $v_{max} \geq v_c$

where the acceleration a_{max} and the velocity v_{max} can be obtained from recorded signals or according to Standard prescriptions, and taking into account the location of the object inside the host building. For a rigid element placed at the ground level, these seismic parameters correspond to *PGA* and *PGV* respectively, while for a rigid element placed at different floor heights, they correspond to *PFA* and *PFV*, respectively.

4 Case studies

This section deals with the seismic assessment of valuable NS elements located in typical RC buildings. In particular, the floor response spectra are determined both with code approaches and with direct generation starting from time-history analyses of the structure. Particular attention is paid to free standing elements, for which both the variations of *PFA* and *PFV* along the building height must be determined. Actually, regarding *PFV* profiles, few research works can be found in literature and, to the authors' knowledge, no recommendations are reported in the international standards.

4.1 Description

Six different case studies are selected, in order to evaluate the influence of the building height and structure type on floor response spectrum trends, in order to study the possible influence of higher modes effects. The selected structures are 3-, 6- and 10-floor buildings, which could be considered representative of the different dynamic behavior respectively of low, medium and high-rise buildings. Furthermore, as highlighted in the introduction section, two different seismic resistant structures are considered for each building height, respectively RC Moment Resisting Frames (*MRF*) with shear-dominated deformed shapes and slender RC Cantilever Walls (*CW*), with flexure-dominated deformed shapes. Concrete class C28/35 and B450C steel rebar type are assumed for the structural elements. The geometries of the frame (*MRF*) and wall (*CW*) buildings are depicted in Figure 2, where each case study is labeled with the acronym "Nr. of floors-structural typology", i.e. 3F-MRF, 3F-CW, 6F-MRF, 6F-CW, 10F-

MRF, 10F-CW.

The case study buildings are designed according to Eurocode 2 [40] and Eurocode 8 [11]. In particular, the seismic design is performed by means of modal response spectrum analysis according to Eurocode 8 [11], assuming for the ULS a response spectrum characterized by a return period T_R = 475 years, ground type A, PGA = 0.3g and behavior factor q=3, which is applicable for both the resisting systems, (see Section 5.2.2.2 of Eurocode 8 [11]). The same q-factor is adopted for both MRF and CW systems in order to obtain a similar level of inelastic demand.

For intermediate floors, the following loads are considered: a permanent load $G_{1,k}$ = 4.0kN/m^2 for structural elements, a permanent load $G_{2,k}$ = 2.4kN/m^2 for non-structural elements and a variable load Q_k = 2.0kN/m^2. For the roof floor: a permanent load $G_{1,k}$ = 4.0kN/m^2 for structural elements, a permanent load $G_{2,k}$ = 2.9kN/m^2 for non-structural elements and a variable load Q_k = 1.2 kN/m^2, due to snow load. The spacing between frames is 6.0m.

Concerning the *MRF* typology, beam and column sections of the 3-story building are respectively 40×50cm and 40×40cm. For the 6-story building the columns sections are 60×60cm at first and second floor, 50×50cm at third and fourth and 40×40cm at the other floors; the beam sections are 40×50cm. Finally, for the 10-story frame, beam sections are 40×70cm and column sections are 50×50cm. The interstory height is 3.5m for 3-story, and 4.0m in the other two cases. The span of the beams is, for all cases, equal to 5.0m. The columns are considered fixed at the base.

As far as the *CW* buildings are concerned, the seismic resistant structure is constituted by RC walls fixed at the base, whereas the vertical loads are carried out by frames, modeled with pinned-pinned columns. For the two RC structural typologies, *MRF* and *CW*, the number and the height of the stories, the height of the building and the story masses are the same. Then, the cross-sections of the walls are designed to obtain, for each *CW* structure, the same fundamental period of the corresponding *MRF* system. The dimensions adopted for the wall

are, therefore, 30×207 cm, 30×375 cm and 30×425 cm respectively for low-, medium- and high-rise buildings, while for the beams and the columns, the same cross sections of the MRF case are adopted.

4.2 Finite element modeling

The numerical investigations for the FRS generation are performed by time-history analyses on detailed finite element (FE) models of each building, by using the OPENSees framework, see [41], [42]. Two different approaches are adopted in the numerical analyses: elastic and inelastic models of the structure. The first ones, used as reference cases, aim to represent the theoretical behavior of the buildings neglecting nonlinear effects during the dynamic response. Nonlinear models, instead, aim to reproduce the nonlinear response of the structures for both medium-high seismic inputs and low-moderate ones, with the latter which do not induce significant structural damage, nor cause yielding of reinforcement bars, but may cause cracking phenomena of some portions of the structural elements.

For the elastic models, elastic 1D elements for beams, columns and walls are adopted, where for walls the Timoshenko's approach is selected. Masses corresponding to structural permanent loads, non-structural permanent loads and live loads are considered as equivalent distributed masses on the beams. For each story, the total vibrating mass is equal to 117.5 x 10^3 kg, 150.0 x 10^3 kg and 60.0 x 10^3 kg respectively for the 3-, 6- and 10-story models. For the CW buildings, the wall is connected by means of a pinned-link, at each floor level, to the frame modelled with pinned-pinned columns.

Table 2 summarizes the first three vibration periods and the correlated effective modal masses (m_{eff}) of each structure considered in the present study.

The inelastic models adopt the same elastic elements for beams, columns and walls used in the elastic models, with lumped flexural plastic hinges, modelled by means of zero-length elements. The trilinear moment-rotation law of the plastic hinges is modeled with the

hysteretic material law described in [41]. Mean values of the material properties are adopted for the definition of the moment-rotation constitutive laws of plastic hinges: for concrete, compression strength f_c = 36MPa and Young modulus E_c = 31.94 GPa; for rebars, yielding stress f_y =500 MPa and Young modulus E_s = 200 GPa. The main points of the moment-rotation backbone curve of the plastic hinges are defined also according to FEMA-273 prescriptions [43], with cracking, yielding and maximum moment in the columns calculated taking the compression axial force due to vertical loads into account. Finally, P-Δ effects are included in the analyses.

4.3 Ground motion selection and dynamic analyses

The first set of 30 horizontal ground motion scaled records are selected to cover a wide range of frequency content, time duration and amplitude, by imposing the spectrum-compatibility criteria prescribed by Eurocode 8 [11] between the average spectrum of the ground motions set and a prescribed target spectrum at ULS. The ULS target spectrum is the same used for the design of structures, i.e. characterized by a return period T_R = 475 years, soil type A and *PGA* = 0.30g. The records, extracted from PEER strong motion database [44], are selected in the range of moment magnitude *Mw* from 5.5 to 8.5, a distance from the source between 10 km and 100 km, different fault mechanisms in absence of strong directivity effects. The main features of the records are reported in Table 3, while Figure 3 shows their elastic pseudo-acceleration response spectra for 5% damping ratio. By means of this first set of ground motions, the behavior of the buildings is investigated in a wide nonlinear range. This set of acceleration ground motions is tagged “0.34g Set”, referring to the average *PGA* of the selected 30 records.

The second set of 30 ground motion records is also selected from PEER strong motion database [44], by adopting the same criteria described above, but imposing the compatibility between the average spectrum of the set of ground motions and a prescribed target spectrum

corresponding to the DLS. The DLS target spectrum, characterized by return period T_R = 50 years, is defined according to Eurocode 8 [11] by assuming a soil type A and *PGA* = 0.1g, typical of the frequent seismic event characterizing the European seismic areas.

By means of this second set of ground motion records, the structures are investigated in a condition of frequent earthquake. Table 4 and Figure 4 summarize, respectively, the main characteristics of the DLS set of 30 records and the elastic pseudo-acceleration 5% damped response spectra, and the comparison between average and target spectrum. This set of acceleration ground motions is tagged "0.12g Set", referring to the average *PGA* of the selected 30 records. The results of the time history analyses with 0.12g Set exhibit a moderate nonlinear behavior of the structures with concrete cracking, but neither high damage nor steel yielding, for all the structural elements.

5 Analysis of the results

5.1 Floor Response Spectra

For all the case studies, the floor response spectra are evaluated by averaging the 30 floor acceleration signals obtained from the time-history analyses considering ξ_a=5%. The two sets of accelerograms are considered, adopting both elastic and inelastic models, and results are compared with those obtained through the spectrum-to-spectrum formulations summarized in section 2. In all the figures, each case study is identified with its acronym (see section 4.1): "Nr. of floors-structure typology". When both typologies are reported in the same figure, the acronyms become: 3F-Buildings, 6F-Buildings and 10F-Buildings.

5.1.1 Numerical results

Figure 5 to Figure 7 show the results obtained by performing elastic and inelastic analyses of the structures, with 0.12g Set and 0.34g Set of time histories. The results are reported for the top level of each buildings and for some floors selected as representative of the structural

response at the low- and mid-height floors. In the same figures, the results obtained by using the spectrum-to-spectrum formulations are also reported, see section 5.1.2. It can be observed that the elastic spectral acceleration corresponding to the first period T_1 of the structure, $S_a(T_1, z)$, is lower than the one corresponding to the second period T_2, except for the top level of the 3-story buildings. In particular, the higher the building, the greater the increase between the spectral value associated with higher modes and $S_a(T_1, z)$. Moreover, the contribution of the higher modes is more evident at the lower floors.

The comparison between elastic and inelastic numerical spectra evidences the effects on FRS of the non linearity of the host structure, which are visible even if the 0.12g Set corresponds to DLS condition and does not imply any yielding phenomena in steel bars or significant damage to structural elements. In particular, the natural periods of the structure increase, the maximum amplification peaks decrease, and the spectral shape becomes smoother with high acceleration demand affecting a wider range of NS period (see also Anajafi and Medina [6]). It is interesting to observe that the first mode spectral peak undergoes the most significant reduction due to non-linearity, while the peak reduction is smaller for the second mode. Therefore, higher modes give greater contributions to the definition of the FRS in the inelastic range, as pointed out, among others, by Petrone et al. for multi-story 2D RC frames [21] As an example, in Figure 5 (3-story buildings, floor 3) it can be observed that, for the *CW* building, the FRS maximum value is associated to the period T_1 in the case of elastic response, and to the period T_2 in the case of inelastic response.

5.1.2 Practical spectrum-to-spectrum approaches

In this section, the numerical floor response spectra described in the previous section are compared with those obtained by the "practical spectrum-to-spectrum approaches" adopted by the Standards and based on simplified formulations (i.e. EC8, MIT19-MRF, ASCE 7-10, NZS 1170.5).

In all the cases represented in Figure 5 and Figure 6, the EC8 formulation, providing a peak amplification in correspondence of T_1, tends to significantly overestimate the numerical results, even when an elastic behavior of the host structure is considered, for NS elements with period T_a close to, or higher than, T_1. The only exception is the case of the top floor of the 3-story buildings, for which the EC8 approach underestimates the floor acceleration obtained by elastic analyses. However, including a moderate non linearity of the host structure (i.e. 0.12g Set of time histories), it gives again conservative results. Finally, the EC8 formulation is not conservative for NS elements with period T_a close to those characterizing the higher modes of the structure. Actually, in this period range, the EC8 approach underestimates the amplification effect, even when a moderate structural non linearity is considered, because, as above mentioned, the role of structural nonlinear behavior is moderate in this spectrum zone. This underestimation is particularly evident at the lower floors and, in general, for the *CW* buildings.

The other practical formulations (i.e. ASCE, NZS and MIT19-MRF) introduce a plateau in the FRS graph, so extending the range of maximum amplification even to periods shorter than the fundamental period T_1. Therefore, these formulations seem to be preferable with respect to EC8 approach and, in general to the approaches with a peak in correspondence of T_1, especially for the study of objects with periods $T_a < T_1$, because they allow capturing, at least partially, the effect of structural higher modes.

Concerning the *MRF* structures, ASCE 7-10 proposal is always on the safe side for 6-story and 10-story buildings, even when compared to the results of the elastic analyses. This is true also for the 3-story building if a moderate non linearity is considered. Similarly, all the other formulations are generally conservative if compared with the inelastic numerical spectrum obtained with 0.12g Set of time histories. On the other hand, with reference to *CW* structures, the practical formulations underestimate in many cases the accelerations of the inelastic numerical spectrum obtained with 0.12g Set of time histories in correspondence of the short

period range.

For both *MRF* and *CW* structures, ASCE 7-10 proposal tends to overestimate the accelerations in the long period range, while NZS formulation, due to its decreasing branch, tends in some cases to become unsafe for periods T_a close to or higher than T_1, especially in the upper part of the higher buildings. On the contrary, NZS proposal is very conservative for rigid objects (i.e. with T_a close to 0).

As far as the ULS spectra are concerned, due to the significant nonlinear behavior of the structures, all the practical approaches become definitively conservative in the high period range (T_a close to or higher than T_1). In the short period range, corresponding to the higher modes, some of the practical approaches may underestimate the inelastic numerical spectra obtained with 0.34g Set of time histories, especially at the lower floor levels and for *CW* structures, as shown for instance in Figure 7 for both the 3 and 6-story buildings.

It is worth noting that the code-based approaches seem more suitable for ULS than DLS spectra. It may be due to the fact that, as explicitly stated by Anajafi and Medina [6] for ASCE 7-10 proposal, the code-based appoaches could be meant to provide the acceleration demand for NS element at the design earthquake (i.e. strong earthquake), when the ordinary buildings are designed to undergo inelastic deformations.

5.1.3 Modal superposition spectrum-to-spectrum approaches

With reference to the time-history analyses carried out with 0.12g Set, the numerical elastic and inelastic floor response spectra described in section 5.1.1 are compared here with the predictions based on the modal superposition approach (i.e. MIT19-Nmodes and MIT19-Simp-Nmodes). Since with low intensity earthquakes the host structure does not exhibit a significant inelastic behavior (only limited cracking phenomena), floor response spectra obtained by using both MIT19-Nmodes and MIT19-Simp-Nmodes formulations are evaluated considering an elastic behavior, namely by introducing the elastic spectrum $S_e(T_i)$ in eq. (5)

and a viscous damping ξ_i=5% in eqs. (7)-(10), together with the natural periods T_i obtained through the modal analysis. The first three vibration modes are considered here.

The results reported in Figure 8 and Figure 9 reveal that these proposals allow capturing the different behavior between *MRF* and *CW* buildings, even in correspondence of the first period of vibration, although it is assumed identical for the two structural typologies. Moreover, this difference increases with decreasing of the story level. The MIT19-Nmodes FRS, assuming β = 0.5 in (6), tends generally to overestimate the peak amplification associated with the fundamental period of the structure, even if compared with the results of elastic numerical analyses. However, in many cases, this formulation underestimates the spectral values between the peaks. The latter tendency still persists even assuming β = 0.4 in eq. (6), as shown for the 6-story building in Figure 10. It is worth noting that the peak amplification associated with the second mode for all the *CW* buildings is underestimated by assuming β = 0.4, even with respect to the numerical floor response spectra obtained with nonlinear analyses.

Regarding the MIT19-Simp-Nmodes formulation, Figure 8 evidences that this proposal well captures the numerical FRS for the 3-story and 6-story *MRF* buildings and that it is always conservative when compared with the results of nonlinear analyses. For the tallest building (i.e. 10-story, Figure 9), this formulation is safe for the upper part of the building, while at lower levels it may underestimate the numerical results.

On the other hand, as far as *CW* buildings are concerned, MIT19-Simp-Nmodes formulation seems to underestimate the numerical FRS at the lower floors and for 6- and 10-story buildings, at every floor, in correspondence of the second natural period. This occurs even if the non linearity of the primary structure is considered.

Finally, a more practice-oriented implementation of these formulations is considered, where only the first vibration mode is taken into account (MIT19-simp-1mode and MIT19-1mode), e.g. [20]. Table 2 summarizes the adopted values of T_1, while the modal shape is assumed

linear along the building height, $\varphi_1(z) = z/h_b$, and the modal participation factor is taken as $\Gamma_1 = 3N/(2N+1)$, where N is the number of the stories. Therefore, with these assumptions, the two formulations give identical predictions for *MRF* and *CW* buildings. Results in Figure 11a show that MIT19-simp-1mode formulation can be conveniently applied to 3- and 6-story buildings only for NS elements with T_a adequately greater than T_2, where adequately means that the lower the placement of NS element within the building, the greater the period T_a should be with respect to T_2. On the other hand, for the tallest buildings (10-story) this formulation seems not applicable at the lower floors, Figure 11b.

From the same figure, it seems evident that also MIT19-Nmodes formulation is not suitable to be applied if only the first vibration mode is considered.

5.2 Profiles of Peak Floor Acceleration – PFA

Due to the importance assumed by *PFA* for free standing objects, as described in Section 3, Figure 12 shows the distribution of *PFA*/*PGA* ratio along the building height, often referred to as the ”in-structure amplification factor”, obtained with nonlinear analyses for 0.12g Set and 0.34g Set of time histories and with elastic analyses (in this case only the results for 0.12g Set are plotted since they are almost identical to those obtained for 0.34g Set). In this figure, the average values of *PFA*/*PGA* are plotted.

The influence of the different lateral resistant systems (*MRF* and *CW*) is now evident due to the different effects of the higher modes. As Figure 12 illustrates, the taller the building, the greater the difference between *MRF* and *CW PFA* profiles. In particular, for 3-story structures with elastic behavior, the *PFA*/*PGA* value tends to increase along the building height regardless of the lateral resistant system, because the response is dominated by the first vibration mode only. For 6- and 10-story buildings, characterized by a higher value of the fundamental period, the *PFA*/*PGA* is no more increasing along the building height and the *CW* shows a typical swinging shape in the upper part of the buildings, in accordance with the

results found, for instance in [8]. Moreover, for a given fundamental period of the structure, *CW* buildings tend to have higher values of *PFA* than the *MRF* ones, especially for the tallest buildings, with the only exception of the floors at level z equal to about $0.8h_b$.

The effect of the non linearity of the host structure provides a reduction of the *PFA*/*PGA* ratio, which is particularly evident in 3-story buildings, as Figure 12 shows. Even a moderate non linearity (0.12g Set) leads to a relevant reduction of the *PGA* amplification. It is worth noting that, for this value of *PGA, MRF* buildings generally do not exhibit acceleration amplification along the building height, in particular the ratio *PFA*/*PGA* is lower than 1 at all the floor levels, except for the top floor of the 3-story building where the amplification is less than 20%. Additionally, for all building typologies, if the nonlinear behavior of the buildings is more pronounced, as in the case of 0.34g Set of time histories, the *PFA*/*PGA* ratios are even smaller. In several cases, they move from values greater than one to values consistently smaller than one, regardless of the first vibration period of the building. Note that it could be interesting to correlate such response to the elongated periods (due to inelastic behavior) and to evaluate as the *PFA/PGA* changes with the period lengthening. This will be investigated in the further development of the research.

Figure 13 shows the comparison between the numerical *PFA*/*PGA* profiles and those predicted by the spectrum-to-spectrum approaches presented in section 2, for the 0.12g Set. The NZS1170.5 is excluded since it is proved to be too conservative for rigid objects in all the case studies, as shown in Figure 5 and Figure 6. It is worth noting that the other "practical approaches" (i.e. ASCE 7-10, EC8 and MIT19-MRF) assume a linear variation of *PFA* along the building height. In particular, the *PFA*/*PGA* ratio predicted by these approaches can be expressed, in general, by the following expression:

$$\frac{PFA(z)}{PGA} = (1 + k_a \cdot z/h_b) \tag{13}$$

where the values of parameter k_a are provided in Table 5 for the different approaches.

As Figure 13 shows, the *PFA*/*PGA* predicted by ASCE 7-10 and EC8 proposals increases along the building height to a maximum value of 3.0 and 2.5, respectively, regardless of the different building typologies. ASCE7-10 proposal is always conservative, for both *MRF* and *CW* buildings, even if an elastic behavior of the host building is assumed. Similarly, the EC8 approach predicts an amplification of *PGA* which is generally safe-sided. Finally, for the *MRF* buildings, MIT19-MRF proposal provides conservative results at all floor levels, even when compared with those obtained by elastic analyses.

Concerning the modal superposition approaches, the *PFA* values predicted by the MIT19-Nmodes formulation is almost identical to the one calculated by the MIT19-Simp-Nmodes proposal. It is worth noting that the results in terms of *PFA* provided by MIT19-Nmodes are independent of the β value assumed in eq. (6). Figure 13 shows the results in terms of *PFA/PGA* considering the first three modes. It is evident that these formulations well capture the *PFA* trend along the building height, especially in the upper part of the building, but they tend to underestimate the *PFA* value even with reference to the inelastic behavior of the structure, in particular at lower floors.

Figure 13 suggests that, for these multimodal formulations, the adjustment recommended by Calvi and Sullivan in [23] for the lower levels can be suitable. Actually, in the quoted paper, the authors recommended the use of SRSS composition rule for the upper levels while, for the lower levels, the adoption of the maximum spectral ordinate between the values obtained by the SRSS composition and the ground response spectrum. This corresponds to assume a lower limit for *PFA*/*PGA* ratio equal to 1.0 for the lower floors.

5.3 Profiles of Peak Floor Velocity – PFV

Similarly to *PFA*, Figure 14 shows the profiles of PFV/PGV ratio along the building height obtained by the elastic and inelastic analyses of the host structures. In this case, the 0.12g Set of time histories is considered, for which a slight nonlinear structural behavior is exhibited,

since it represents the most conservative case for evaluating the seismic demand, especially in the case of valuable elements.

It is evident that, differently from *PFA*, *PFV* increases quite regularly along the building height for all the case studies, regardless of the lateral resistant typologies and the total height of the building. For the *MRF* buildings, this increase is almost linear. In addition, the difference between the *PFV* amplifications for the two structural typologies is generally quite limited, with some exceptions at the top floors (maximum difference equal to 27% for the 3-story building). The *MRF* buildings have generally the largest amplification, except for some floors at the top.

The effect of a slight non linearity of the host structure (i.e. concrete cracking without steel yielding) generally provides a reduction of the *PFV*/*PGV* ratio. The greater the distance from the ground level, the higher the difference between the *PFV*/*PGV* nonlinear profile and the linear one, that is the effect of non-linearity is more evident in the upper floors of the buildings.

6 Stability Charts

As described in Section 3, the seismic safety assessment of free standing NS elements requires the check of the limit equilibrium with reference to the possible different rigid motions, i.e. rocking, overturning, sliding. With the hypothesis that the friction coefficient between the object and the support surface is sufficient to avoid the occurrence of a sliding motion before rocking, an operational and effective tool to evaluate the stability of the elements against rocking and overturning is represented by the “stability charts”.

In this work, based on the case studies described in Section 4, stability charts are created adopting the criteria expressed in eq. (12) and considering the floor acceleration and velocity evaluated in Sections 5.2 and 5.3. The charts allow to quickly assess the safety of an object given its geometric characteristics *B* and *H*, the seismicity of the site, and its localization at

the different floors of the host building.

Figure 15 shows the stability chart referred to the ground floor for the seismic demand corresponding to 0.12g Set (*PGA* = 0.12 g and *PGV* = 0.091 m/s – average of the 30 DLS signals). According to the criterion reported in eq. (12), the region above the line *B/H = PGA* corresponds to the stability condition, the region between the rocking line condition and the overturning curve obtained from eq. (11) - setting $v_c = PGV$ - corresponds to the rocking condition and the region under the overturning curve corresponds to the overturning condition. As an example, Figure 16 shows the charts referred to 3rd floor and top floor level of the 6-story building using *PFA* and *PFV* obtained from the numerical simulations. The comparison between *MRF* and *CW* buildings reveals the difference in the stability conditions for the two typologies of structures, in particular in terms of rocking tendency. The stability region for *MRF* buildings is generally wider than that of *CW* buildings. Moreover, the same figure shows the effect of considering the non linearity of the host structure, with the widening of the stability region.

Concerning the rocking occurrence, particularly relevant for the valuable NS elements, Figure 17 reports the critical value of the ratio *B/H* divided by *PGA*/*g* at different floor levels of the three case studies. Given a value of *PGA*, which characterizes the seismicity of the site, the charts provide, for each floor, the limit value of the *B/H* ratio to guarantee the stability condition of the NS element. In Figure 17, the *PFA* predicted by the analysed spectrum-to-spectrum approaches are also presented.

In this work, a more complete operative tool for the seismic assessment of free standing NS elements is also proposed, where the overturning limit condition is included as a function of *H*. This chart allows evaluating the stability condition of a free standing NS element as a function of its geometrical characteristics *B* and *H,* the seismicity of the site (in terms of *PGA*, and *PGV*), the structural typology (i.e. *MRF* or *CW* buildings) and the placement of the element along the height of the building (z/h_b).

Figure 18 shows this chart applied to the case studies, where *PGV* is obtained by adopting the relationship proposed by the Italian NTC Standards, i.e. $PGV = 0.16\, PGA\, T_c$, with T_c = 0.25s according to type 2 spectrum of Eurocode 8. Concerning the amplification of *PFA* along the building height, the *PFA*/*PGA* ratio predicted by the European codes MIT19-MRF and EC8 proposals are adopted. Note that the first one can be profitably used only for frame buildings, while EC8 proposal can be used also for wall buildings, with some caution for the mid floor levels. However, it is worth noting that, for real buildings where a slight nonlinear response (corresponding to concrete cracking without steel yielding) is usually exhibited, both the EC8 and MIT19-MRF profiles provide reliable predictions.

The use of the chart is twofold. Given a value of *PGA,* this chart allows obtaining the maximum floor level at which an object, characterized by *B* and *H*, can be located in order to avoid overturning or rocking. As an example, following the red path reported in Figure 18, starting from the point A of the chart on the right, (*B/H*)/(*PGA*/g)=0.8, for an object with height *H*=0.25m, the *PFA/PGA* limit for the overturning condition is 1.48. The corresponding maximum floor level (z/h_b) for avoiding overturning is equal to 0.32 and 0.48, depending on the adopted proposals for *PFA/PGA* ratio prediction. Furthermore, the red path indicated in Figure 18 can also be used backward: for a given floor level and a given value of *PGA*, this chart allows to determine the minimum value of *B* that an object (characterized by fixed *H*) must have in order to avoid overturning, and the minimum value of *B/H* ratio in order to avoid rocking. It is worth noting that, for a given value of *B/H*, the greater the dimension *H* of the object, the more stable the object is, with reference to overturning, e.g. [14].

Finally, to create this chart, a *PFV*/*PGV* profile variation with height has to be assigned. In this paper, a linear variation of *PFV*/*PGV* with height is assumed, similar to that adopted by the practical approaches for *PFA/PGA,* eq. (13):

$$\frac{PFV(z)}{PGV} = (1 + k_v \cdot z/h_b) \tag{14}$$

where, as a first approximation, the coefficient k_v is assumed equal to k_a of eq. (13), namely k_v= 1 (for MRF, consistent with MIT19-MRF approach), k_v= 1.5 (for both MRF and CW consistent with EC8). Figure 19 shows the adopted proposal of the *PFV*/*PGV* profile compared with the *PFV/PGV* obtained by numerical analyses (elastic and inelastic with 0.12g Set of time histories) presented in Section 5.3.

Note that the proposed linear relationship (14) for *PFV*/*PGV* demonstrated to be conservative if a slight non linearity is considered for both MRF buildings with k_v= 1.0, and for CW buildings. On the other hand, for MRF buildings the k_v= 1.5 assumption is conservative even if the structure remains in elastic range.

7 Conclusions

In the present paper, the seismic assessment of valuable NS elements, i.e. NS elements characterized by high value in terms of economic, cultural or strategic sense, is dealt with. Particular attention is paid to the evaluation of the seismic demand using the Floor Response Spectrum (FRS) approach. Indeed, the knolewdge of the seismic demand at the different floor levels could have a significant impact on the best localization of valuable elements in a building.

The results of a parametric study on floor response spectra obtained via elastic and nonlinear numerical modeling of RC buildings are presented. Three different heights (3, 6 and 10 floors) and two different typologies of seismic resistant structures (*MRF* and *CW*) are considered, subject to two sets of 30 horizontal ground motions records, compatible with the spectrum at Ultimate Limit State (ULS) and at Damage Limitation State (DLS). In order to investigate the effect of different mode shapes and of the higher modes of the host structure on the FRS evaluation, the two building typologies are designed to have the same first mode vibration period. The numerical floor response spectra are compared with those obtained with the most commonly used formulations proposed by national and international codes and

Standards (i.e. Eurocode 8, ASCE 7-10, NZS 1170.5, MIT19-Commentary of Italian Standard NTC2018). It is worth noting that the valuable NS elements should be protected not only in the case of strong earthquakes, but in particular, in the case of low-moderate ones, which usually cause only cracking phenomena in the structural elements, but may induce unacceptable damage to the NS elements.

One of the main outcomes of this parametric study concerns the vulnerability of objects characterized by short vibration periods (close to those of higher modes of the primary structure) in particular when they are located at the lower part of *CW* structures. Actually, for this type of building typology and for these objects, floor spectral accelerations tend to be high and strongly influenced by the higher modes, also when the structural non linearity is accounted for. As an example, the results of nonlinear analysis for 6- story *CW* buildings for low-moderate earthquakes (SLD) show that the spectral acceleration for a period close to the second period of the primary structure can reach 7.0 times PGA at the second floor. In these conditions, the analytical spectrum-to-spectrum approaches, used in this work for comparison purposes, may significantly underestimate the acceleration amplification effect due to the host structure oscillation, so demonstrating to be not always conservative. In the above mentioned 6- story *CW* buildings case, the value recommended by EC8 is lower than 2.0 times PGA, while according to ASCE 7-10 and NZS 1170.5 this value reaches 5.0 times PGA at most. Moreover, it is worth noting that the practical approaches do not allow capturing the different behavior between *MRF* and *CW* buildings in the whole period range, which is, on the contrary, well captured by the modal superposition spectrum-to-spectrum approaches even if they underestimate in some cases the spectral values between the peaks. From this parametric study, it can be underlined that the spectrum-to-spectrum approaches can be effectively applied to assess the acceleration demand of NS elements with a period equal to or higher than the fundamental period T_1 of the primary structure, while attention must be paid for elements with period lower than T_1 , especially for CW buildings in the lower floors.

As far as free standing objects are concerned, which represent a significative part of the category of valuable NS elements, the evaluation of Peak Floor Acceleration and Velocity (*PFA* and *PFV*) becomes crucial to assess the rocking and overturning stability conditions. Regarding *PFA*, all the practical approaches provide conservative results at all floor levels of the host structure, even when compared with the numerical results obtained by elastic analysis, which of course indicate higher accelerations with respect to those obtained from a nonlinear analysis. Therefore, for the seismic vulnerability assessment of freestanding objects the value of *PFA/PGA* predicted by the practical approaches (i.e. EC8, MIT19-MRF, ASCE 7-10 and NZS 1170.5) may be safely used for real buildings, that in case of low-moderate earthquakes show at least a moderate nonlinear behaviour. On the contrary, the modal superposition approaches tend to underestimate the *PFA* especially at lower floors of *CW* buildings, even when the inelastic behavior of the structure is considered. However, these approaches capture quite well the *PFA*/*PGA* trend along the building height (differently from the practical approaches which assume a linear profile of *PFA/PGA* along the building, regardless of the structural typology), evidencing also that the *CW* buildings tend to have higher values of *PFA* than the *MRF* ones.

Concerning the evaluation of *PFV*, to the authors' knowledge, no recommendations can be found in national and international Standards. For all the proposed case studies, *PFV* increases quite regularly along the building height without a significant difference between the two structural typologies. Therefore, in this work, a linear *PFV/PGV* variation with height is suggested as a first approximate proposal of the floor velocity if the seismic safety of free standing elements against overturning must be assessed.

On the basis of these results, stability charts are proposed in this paper as operational and effective tools for large-scale seismic vulnerability assessment of free standing objects located inside a building. These charts allow evaluating the stability conditions against rocking and overturning, using limited number of information about the geometry of the object, its

placement inside the building and the seismicity of the site. These tools can be used for example to obtain the minima dimensions of the support base of an object, as well as to identify the best location inside the building to increase its safety, with respect to both rocking and overturning conditions. The particular features of valuable NS elements imply that even a small damage level may cause significative losses, so making often the rocking occurrence the most critical phenomenon.

In the future steps of this research, a higher number of case studies, including also 3D-structures will be considered and analysed, together with a statistical analysis of numerical results, in order to obtain more general indications.

8 Acknowledgment

The research project reported in this paper was conducted thanks to financial support from DPC-ReLUIS 2019-2021, Italy.

9 List of abbreviations

ASCE 7-10	ASCE Standard ASCE/SEI 7-10
CW	Cantilever Wall
DLS	Damage Limitation State
EC8	Eurocode 8
FRS	Floor Response Spectrum
HVAC	Heating, Ventilation and Air conditioning
MIT19	Ministry of Italian Infrastructures and Transportation, Commentary of Italian Building Standard (2019)
MIT19-MRF	Simplified FRS formulation for Moment Resisting Frame (MRF) buildings according to MIT19

MIT19-Nmodes	Multimodal FRS formulation according to MIT19
MIT19-Simp-Nmodes	Simplified multimodal FRS formulation according to MIT19, calculated with N vibrational modes
MIT19-Simp-1mode	Simplified multimodal FRS formulation according to MIT19, calculated with first vibrational mode
MRF	Moment Resisting Frame
NS	Nonstructural
NZS 1170.5	New Zealand Standard (1170.5:2004)
PFA	Peak Floor Acceleration
PFV	Peak Floor Velocity
PGA	Peak Ground Acceleration
PGV	Peak Ground Velocity
RC	Reinforced Concrete
SRSS	Square Root Sum of Squares
ULS	Ultimate Limit State
2D	Two dimensional
3F-CW	3 Floors buildings- Cantilever Wall structural typology
3F-MRF	3 Floors buildings- Moment Resisting Frame structural typology
6F-CW	6 Floors buildings- Cantilever Wall structural typology
6F-MRF	6 Floors buildings- Moment Resisting Frame structural typology
10F-CW	10 Floors buildings- Cantilever Wall structural typology
10F-MRF	10 Floors buildings- Moment Resisting Frame structural typology

10 References

[1] Filiatrault A, Sullivan T. Performance-based seismic design of nonstructural building components: The next frontier of earthquake engineering. Earthq Eng Eng Vib

2014;13:17–46. doi:10.1007/s11803-014-0238-9.

[2] Applied Technology Council. Seismic analysis, design, and installation of nonstructural components and systems - background and recommendations for future work. Gaithersburg, MD: 2017. doi:10.6028/NIST.GCR.17-917-44.

[3] Santarsiero G, Di Sarno L, Giovinazzi S, Masi A, Cosenza E, Biondi S. Performance of the healthcare facilities during the 2016–2017 Central Italy seismic sequence. Bull Earthq Eng 2018:1–27. doi:10.1007/s10518-018-0330-z.

[4] Di Sarno L, Yenidogan C, Erdik M. Field evidence and numerical investigation of the Mw = 7.1 October 23 Van, Tabanli and the Mw > 5.7 November earthquakes of 2011. Bull Earthq Eng 2013;11:313–46. doi:10.1007/s10518-012-9417-0.

[5] Miranda E., Taghavi S. Estimation of Seismic Demands on Acceleration-sensitive Nonstructural Components in Critical Facilities. Proc. Semin. Seism. Des. Performance, Retrofit Nonstructural Components Crit. Facil. ATC 29−2, Newport Beach, CA, 2003, p. 347−360.

[6] Anajafi H, Medina RA. Evaluation of ASCE 7 equations for designing acceleration sensitive nonstructural components using data from instrumented buildings. Earthq Eng Struct Dyn 2018;47:1984–1984. doi:10.1002/eqe.3057.

[7] Vukobratović V, Fajfar P. A method for the direct estimation of floor acceleration spectra for elastic and inelastic MDOF structures. Earthq Eng Struct Dyn 2016;45:2495–511. doi:10.1002/eqe.2779.

[8] Taghavi, S., Miranda E. Probabilistic seismic assessment of floor acceleration demands in multistory buildings. Dep Civ Environ Eng Stanford Univ Rep No 162 2006.

[9] Adam C, Furtmüller T, Moschen L. Floor Response Spectra for Moderately Heavy Nonstructural Elements Attached to Ductile Frame Structures. In: Papadrakakis M., Fragiadakis M. P V., editor. Comput. Methods Earthq. Eng., Springer, Dordrecht; 2013, p. 69–89. doi:10.1007/978-94-007-6573-3_4.

[10] Villaverde R. Seismic Analysis and Design of Nonstructural Elements. In: Y VB, Bertero, editors. Earthq. Eng. from Eng. Seismol. to Perform. Based Eng., CRC Press LLC: Boca Raton, FL; 2004, p. 48.

[11] Eurocode 8: EN 1998-1:2004. Design of structures for earthquake resistance. Part 1-1: General rules – Seismic actions and general requirements for structures. Brussels,

Belgium: 2004.

[12] ASCE/SEI Standard 7−10. Minimum Design Loads for Buildings and Other Structures. Reston, VA: American Society of Civil Engineers; 2010.

[13] NZS 1170.5 New Zealand Code. Assessment and improvement of the structural performance of buildings in earthquake. Recommendations of a NZSEE Study Group. Wellington, New Zealand: New Zealand Society- for Earthquake Engineering,; 2006.

[14] Berto L, Rocca I, Saetta A. Vulnerability assessment methods for rocking and overturning of free standing elements. Soil Dyn Earthq Eng 2018;110. doi:10.1016/j.soildyn.2018.02.010.

[15] Sullivan TJ, Calvi PM, Nascimbene R. Towards improved floor spectra estimates for seismic design. Earthquakes Struct 2013;4:109–32. doi:10.12989/eas.2013.4.1.109.

[16] Medina RA, Sankaranarayanan R, Kingston KM. Floor response spectra for light components mounted on regular moment-resisting frame structures. Eng Struct 2006;28:1927–40. doi:10.1016/J.ENGSTRUCT.2006.03.022.

[17] Vukobratović V, Fajfar P. Code-oriented floor acceleration spectra for building structures. Bull Earthq Eng 2017;15:3013–26. doi:10.1007/s10518-016-0076-4.

[18] Singh AK, Ang A.-S. Stochastic prediction of maximum seismic response of light secondary systems. Nucl Eng Des 1974;29:218–30. doi:10.1016/0029-5493(74)90124-1.

[19] Vukobratović V, Fajfar P. A method for the direct determination of approximate floor response spectra for SDOF inelastic structures. Bull Earthq Eng 2015;13:1405–24. doi:10.1007/s10518-014-9667-0.

[20] Degli Abbati S, Cattari S, Lagomarsino S. Theoretically-based and practice-oriented formulationsfor the floor spectra evaluation. Earthquakes Struct 2018;15:565. doi:10.12989/EAS.2018.15.5.565.

[21] Petrone C, Magliulo G, Manfredi G. Floor response spectra in RC frame structures designed according to Eurocode 8. Bull Earthq Eng 2016;14:747–67. doi:10.1007/s10518-015-9846-7.

[22] Lagomarsino S. Seismic assessment of rocking masonry structures. Bull Earthq Eng 2015;13:97–128. doi:10.1007/s10518-014-9609-x.

[23] Calvi PM, Sullivan TJ. Estimating floor spectra in multiple degree of freedom systems. Earthquakes Struct 2014;7:17–38. doi:10.12989/eas.2014.7.1.017.

[24] Petrone C, Magliulo G, Manfredi G. Seismic demand on light acceleration-sensitive nonstructural components in European reinforced concrete buildings. Earthq Eng Struct Dyn 2015;44:1203–17. doi:10.1002/eqe.2508.

[25] MIT - Ministro delle infrastrutture e dei trasporti Circ. C.S.Ll. 21 gennaio 2019 n. 7. Istruzioni per l'applicazione dell'«Aggiornamento delle "Norme tecniche per le costruzioni"» di cui al decreto ministeriale 17 gennaio 2018. 2019.

[26] Fathali S, Lizundia B. Evaluation of current seismic design equations for nonstructural components in tall buildings using strong motion records. Struct Des Tall Spec Build 2011;20:30–46. doi:10.1002/tal.736.

[27] Housner GW. THE BEHAVIOR OF INVERTED PENDULUM STRUCTURES DURING EARTHQUAKES. Bull Seismol Soc Am 1963;53:403–17.

[28] Ishiyama Y. Motions of rigid bodies and criteria for overturning by earthquake excitations. Earthq Eng Struct Dyn 1982;10:635–50. doi:10.1002/eqe.4290100502.

[29] Ishiyama Y. Motions of rigid bodies and criteria for overturning by earthquake excitations. Bull New Zeal Soc Earthq Eng 1984;17:24–37.

[30] Lam NTK, Gad EF. Overturning of non-structural components in low-moderate seismicity region. EJSE Spec Issue Earthq Eng Low Moderate Seism Reg Southeast Asia Aust 2008:121–32.

[31] Yim C-S, Chopra AK, Penzien J. Rocking response of rigid blocks to earthquakes. Earthq Eng Struct Dyn 1980;8:565–87. doi:10.1002/eqe.4290080606.

[32] Zhang J, Makris N. Rocking response of free-standing blocks under cycloidal pulses. J Eng Mech 2001;127:473–83. doi:10.1061/(ASCE)0733-9399(2001)127:5(473).

[33] DeJong MJ. Amplification of rocking due to horizontal ground motion. Earthq Spectra 2012;28:1405–21. doi:10.1193/1.4000085.

[34] Kounadis AN. Parametric study in rocking instability of a rigid block under harmonic ground pulse: A unified approach. Soil Dyn Earthq Eng 2013;45:125–43. doi:10.1016/J.SOILDYN.2012.10.002.

[35] Petrone C, Di Sarno L, Magliulo G, Cosenza E. Numerical modelling and fragility

assessment of typical freestanding building contents. Bull Earthq Eng 2017;15:1609–33. doi:10.1007/s10518-016-0034-1.

[36] Purvance MD, Anooshehpoor A, Brune JN. Freestanding block overturning fragilities: Numerical simulation and experimental validation. Earthq Eng Struct Dyn 2008;37:791–808. doi:10.1002/eqe.789.

[37] Kafle B, Lam NTK, Gad EF, Wilson J. Displacement controlled rocking behaviour of rigid objects. Earthq Eng Struct Dyn 2011;40:1653–69. doi:10.1002/eqe.1107.

[38] Di Sarno L, Magliulo G, D'Angela D, Cosenza E. Experimental assessment of the seismic performance of hospital cabinets using shake table testing. Earthq Eng Struct Dyn 2019;48:103–23. doi:10.1002/eqe.3127.

[39] Berto L, Favaretto T, Saetta A, Antonelli F, Lazzarini L. Assessment of seismic vulnerability of art objects: The "Galleria dei Prigioni" sculptures at the Accademia Gallery in Florence. J Cult Herit 2012;13. doi:10.1016/j.culher.2011.06.005.

[40] Eurocode 2 EN 1992-1-1. Design of concrete structures - Part 1-1 : General rules and rules for buildings. Brussels, Belgium: 2004.

[41] McKenna F, Scott MH, Fenves GL. Nonlinear Finite-Element Analysis Software Architecture Using Object Composition. J Comput Civ Eng 2010;24:95–107. doi:10.1061/(ASCE)CP.1943-5487.0000002.

[42] McKenna F. OpenSees: A Framework for Earthquake Engineering Simulation. Comput Sci Eng 2011;13:58–66. doi:10.1109/MCSE.2011.66.

[43] FEMA-273. NEHRP guidelines for the seismic rehabilitation of buildings: FEMA 273. Federal Emergency Management Agency. Washington, DC: 1997.

[44] PEER (Pacific Earthquake Engineering Research Center). Structural Performance Database Website,"http://nisee.berkeley.edu/spd/index.html." 2003.

FIGURE LEGEND

Figure 1: Coefficients according to NZS1170.5 for the NZS definition: (a) $C_{Hi}(z)$; (b) $C_i(T)$.

Figure 2: Geometries of the Moment Resisting Frame (*MRF)* and Cantilever Walls (*CW)* case studies.

Figure 3: 0.34g Set. Elastic pseudo-acceleration response spectra for 5% damping ratio: 30 ground motion records (grey lines), average spectrum (black line) and target spectrum (red line).

Figure 4: 0.12g Set. Elastic pseudo-acceleration response spectra for 5% damping ratio: 30 ground motion records (grey lines), average spectrum (black line) and target spectrum (red line).

Figure 5: 0.12g Set: (a) 3-story buildings; (b) 6-story buildings. Numerical floor response spectra obtained by elastic and inelastic analyses compared with those obtained by the practical spectrum-to-spectrum approaches (EC8, MIT19-MRF, ASCE 7-10, NZS 1170.5).

Figure 6: 0.12g Set: 10-story buildings. Numerical floor response spectra obtained by elastic and inelastic analyses compared with those obtained by the practical spectrum-to-spectrum approaches (EC8, MIT19-MRF, ASCE 7-10, NZS 1170.5).

Figure 7: 0.34g Set: (a) 3-story buildings; (b) 6-story buildings. Numerical floor response spectra obtained by elastic and inelastic analyses compared with those obtained by the practical spectrum-to-spectrum approaches (EC8, MIT19-MRF, ASCE 7-10, NZS 1170.5).

Figure 8: 0.12g Set: (a) 3-story buildings; (b) 6-story buildings. Numerical floor response spectra obtained by elastic and inelastic analyses compared with those obtained from the modal superposition spectrum-to-spectrum approaches (MIT19-Nmodes

Figure 19 Proposal of a *PFV*/*PGV* profile compared with those obtained by elastic and inelastic analyses with 0.12g Set of time histories: (a) *CW* buildings; (b) *MRF* buildings.

TABLE LEGEND

Table 1 Parameters a, b, a_p of equation (10) (Table C7.2.II, Commentary of Italian Standard, [25]).

Table 2 Periods of vibration and effective modal masses (m_{eff}) for the case study buildings.

Table 3 0.34g Set: Ultimate Limit State (ULS) ground motion characteristics.

Table 4 0.12g Set: Damage Limitation State (DLS) ground motion characteristics.

Table 5 Value of k_a for the different practical spectrum-to-spectrum approaches.

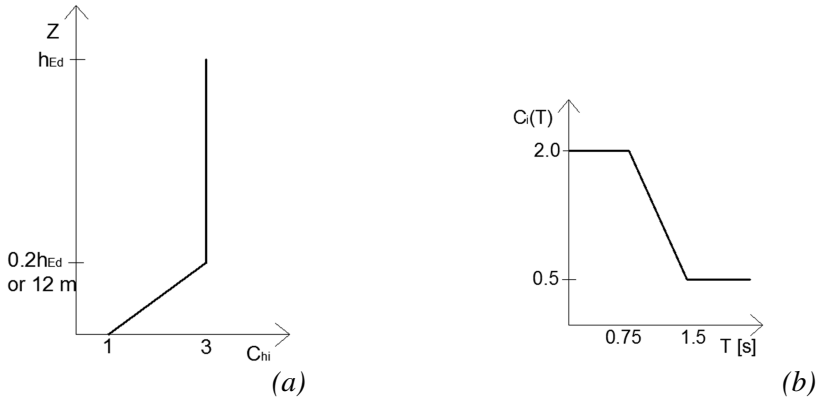

Figure 1: Coefficients according to NZS1170.5 for the FRS definition: (a) $C_{Hi}(z)$; (b) $C_i(T)$.

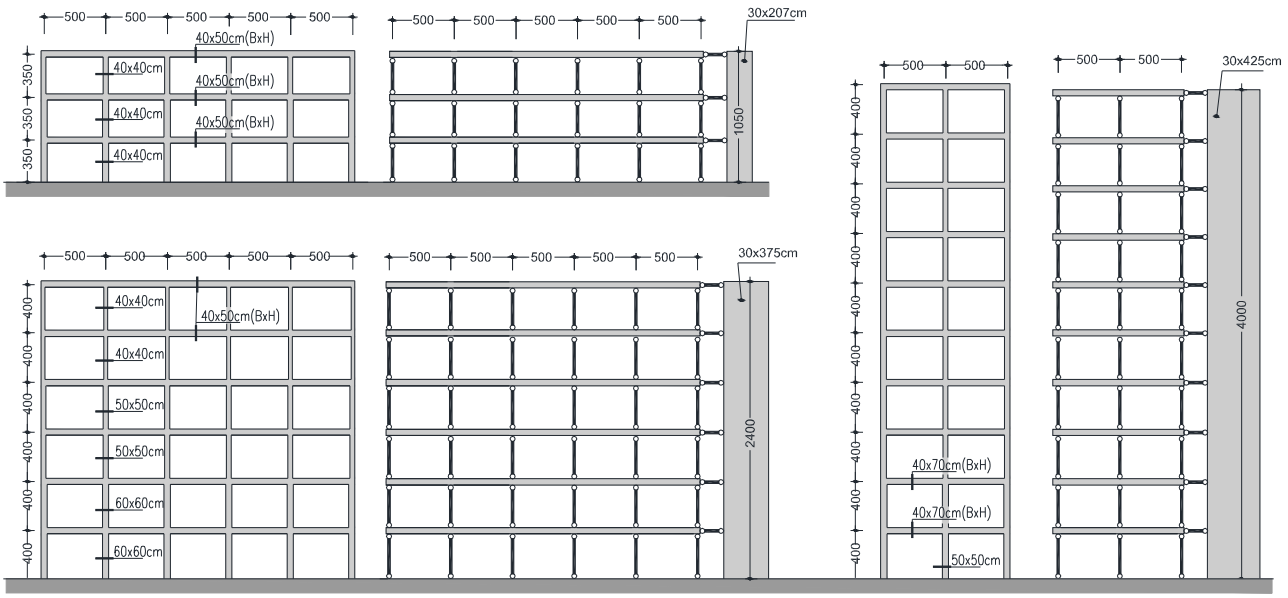

Figure 2: Geometry of the Moment Resisting Frame (*MRF)* and Cantilever Walls (*CW)* case studies.

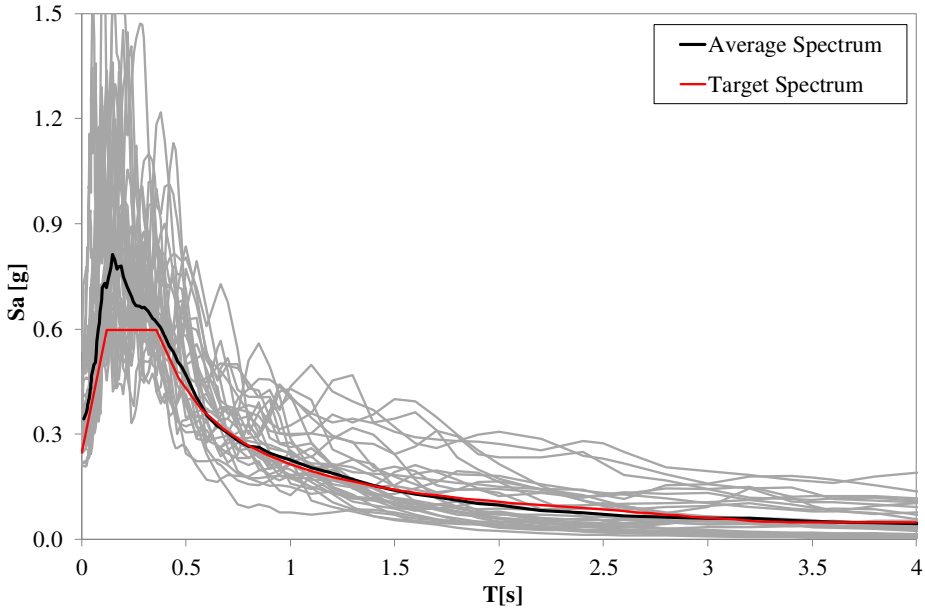

Figure 3: 0.34g Set. Elastic pseudo-acceleration response spectra for 5% damping ratio: 30 ground-motion records (grey lines), average spectrum (black line) and target spectrum (red line).

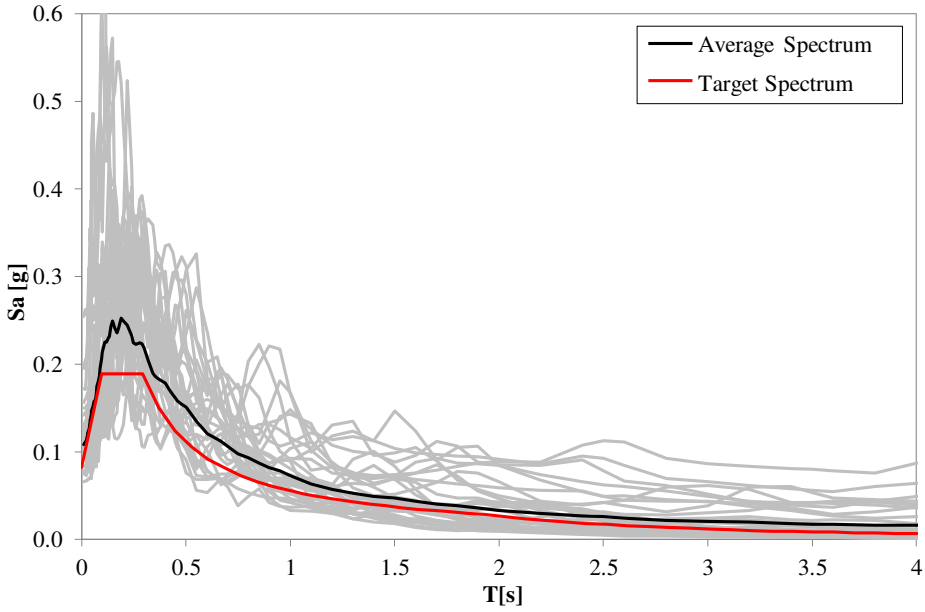

Figure 4: 0.12g Set. Elastic pseudo-acceleration response spectra for 5% damping ratio: 30 ground-motion records (grey lines), average spectrum (black line) and target spectrum (red line).

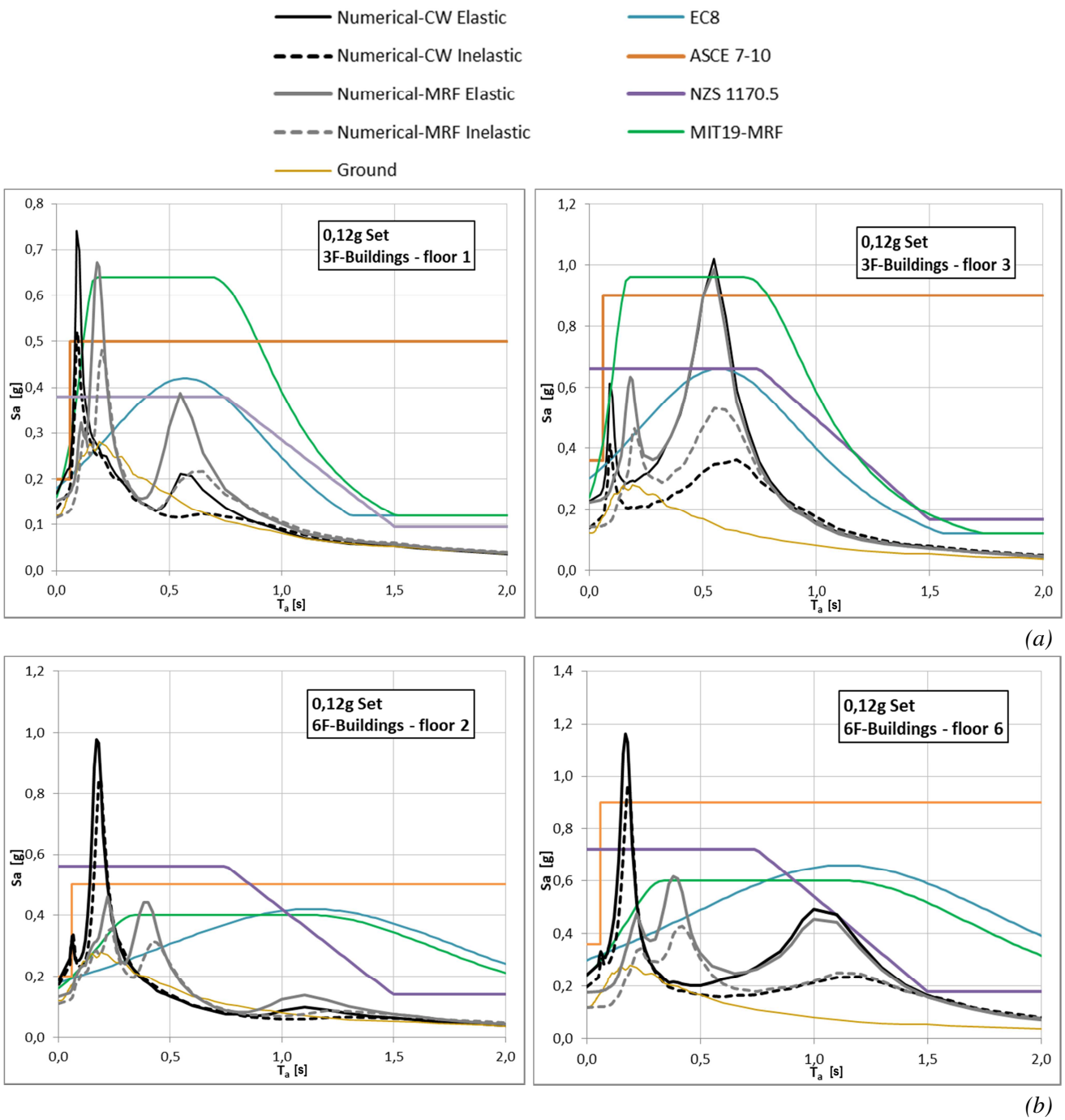

Figure 5: 0.12g Set: (a) 3-story buildings; (b) 6-story buildings. Numerical floor response spectra obtained by elastic and inelastic analyses compared with those obtained by the practical spectrum-to-spectrum approaches (EC8, MIT19-MRF, ASCE 7-10, NZS 1170.5).

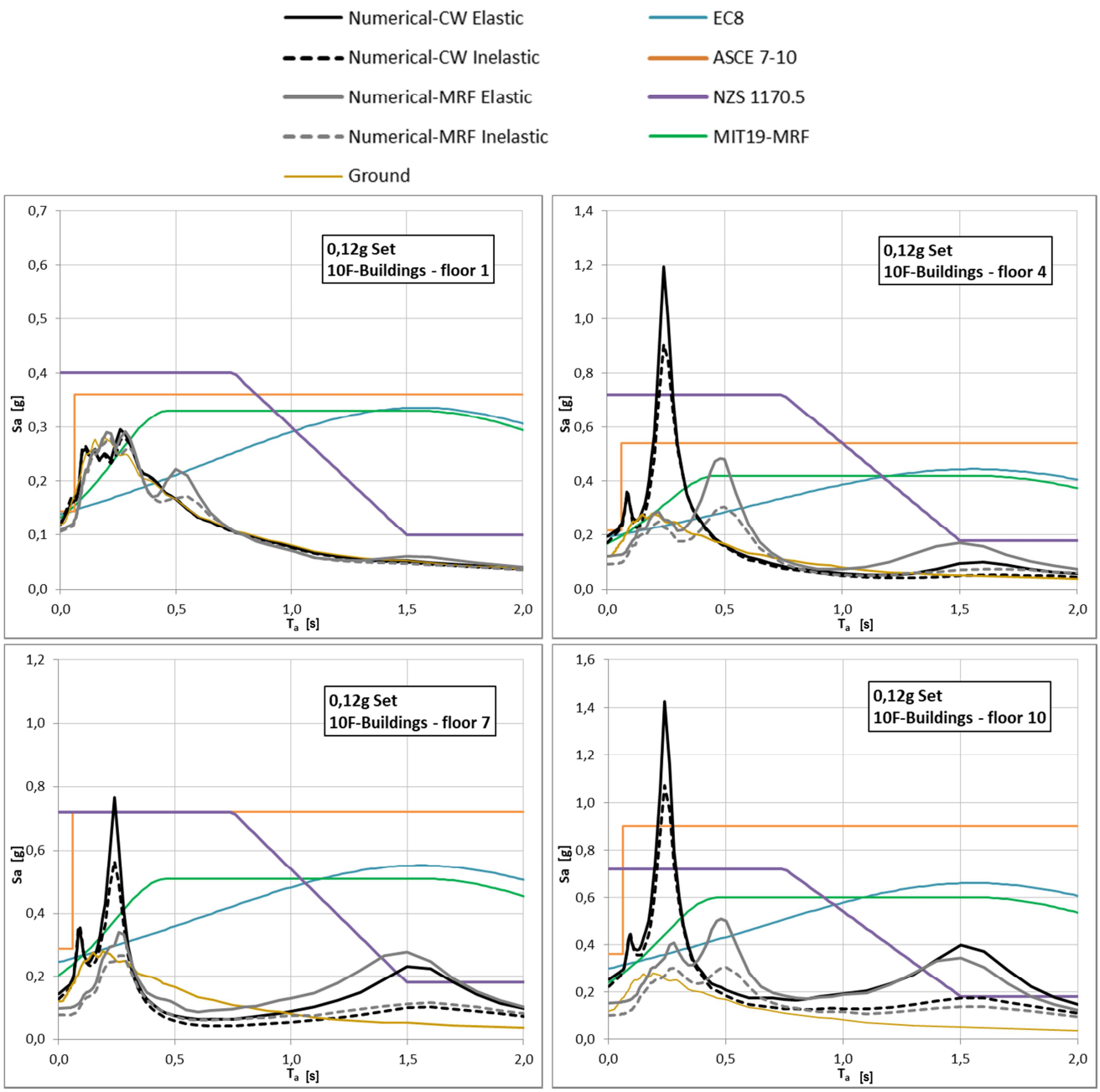

Figure 6: 0.12g Set: 10-story buildings. Numerical floor response spectra obtained by elastic and inelastic analysis compared with those obtained by the practical spectrum-to-spectrum approaches (EC8, MIT19-MRF, ASCE 7-10, NZS 1170.5).

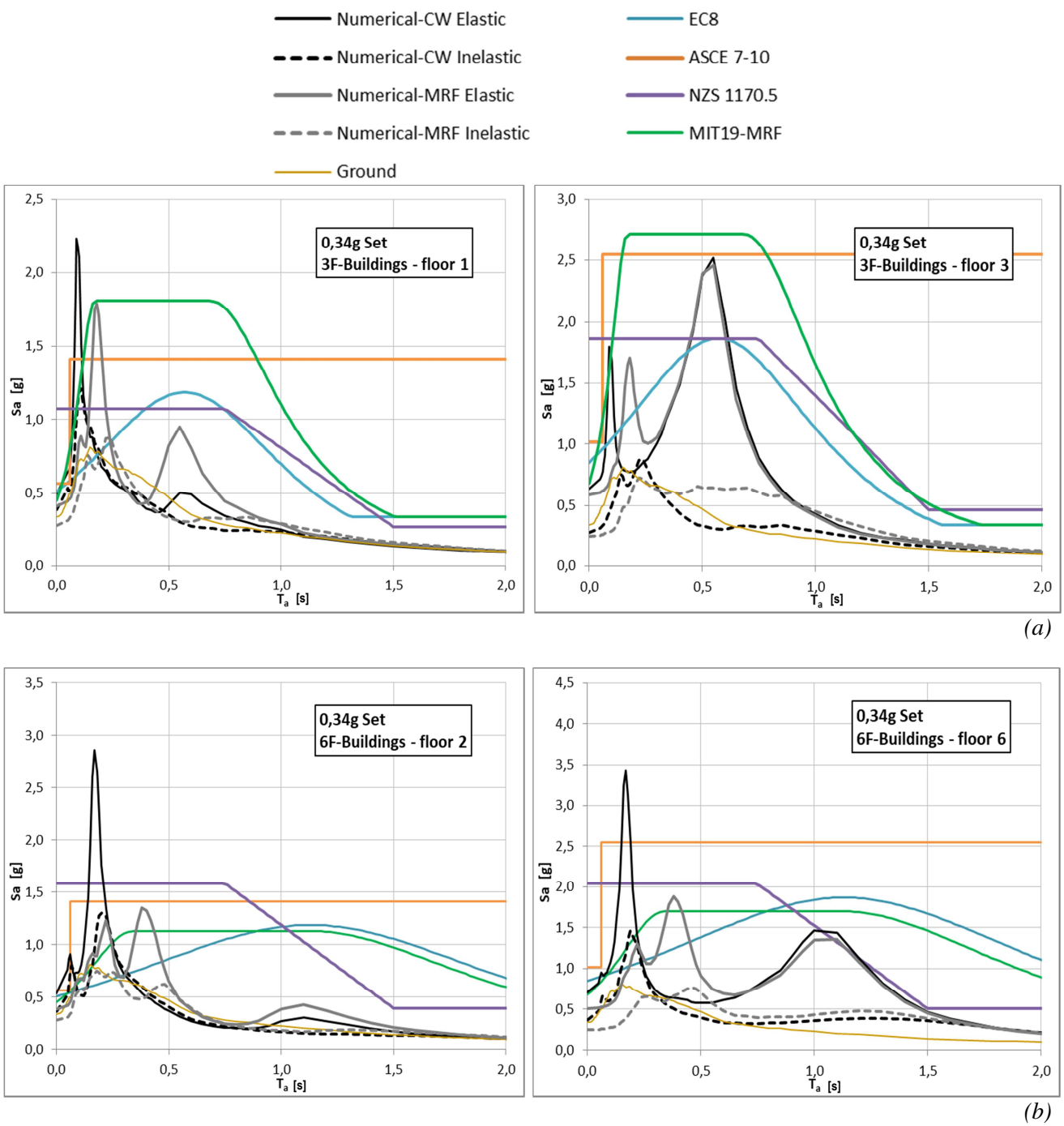

Figure 7: 0.34g Set: (a) 3-story buildings; (b) 6-story buildings. Numerical floor response spectra obtained by elastic and inelastic analyses compared with those obtained by the practical spectrum-to-spectrum approaches (EC8, MIT19-MRF, ASCE 7-10, NZS 1170.5).

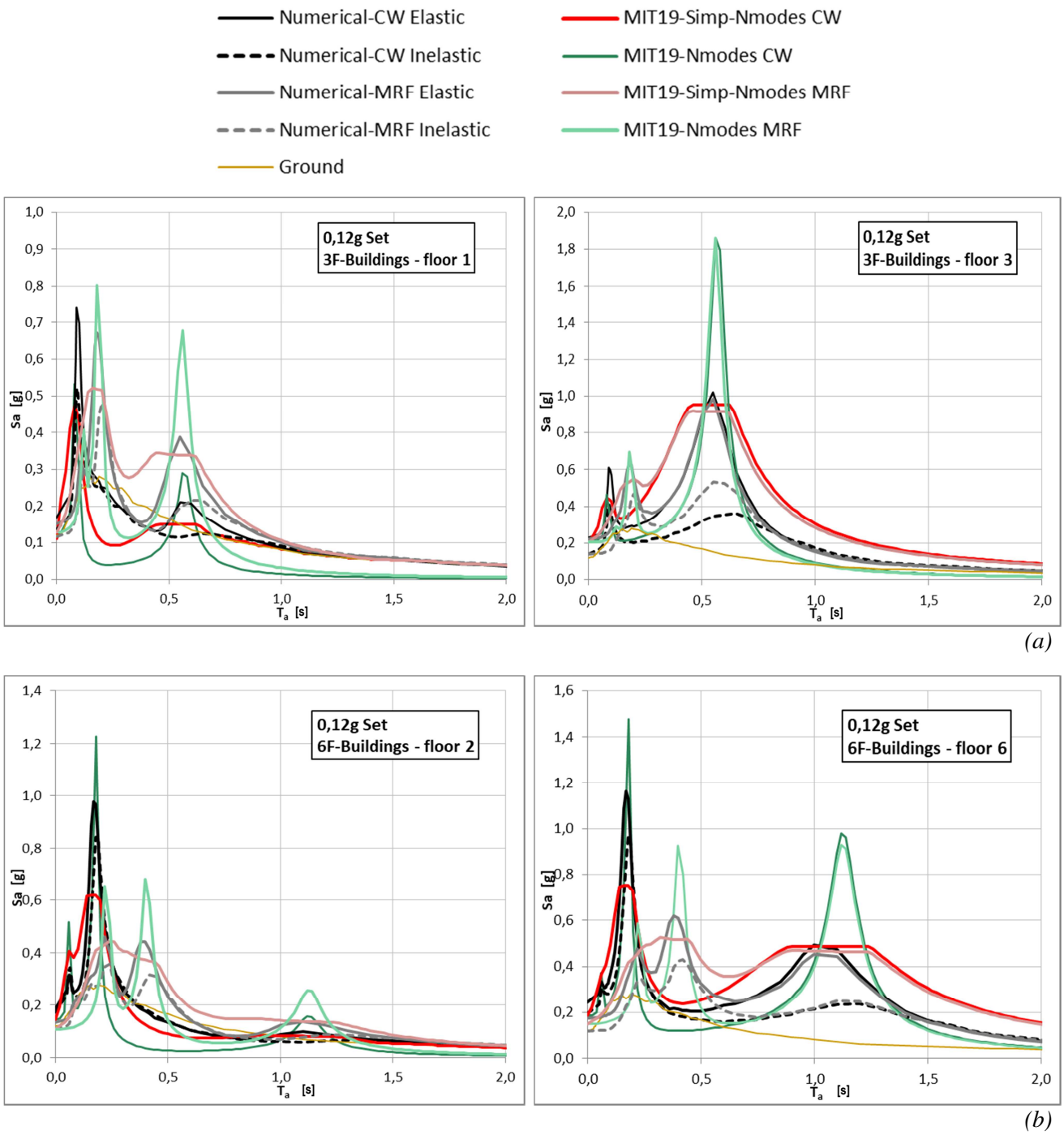

Figure 8: 0.12g Set: (a) 3-story buildings; (b) 6-story buildings. Numerical floor response spectra obtained by elastic and inelastic analysis compared with those obtained from the modal superposition spectrum-to-spectrum approaches (MIT19-Nmodes and MIT19-Simp-Nmodes).

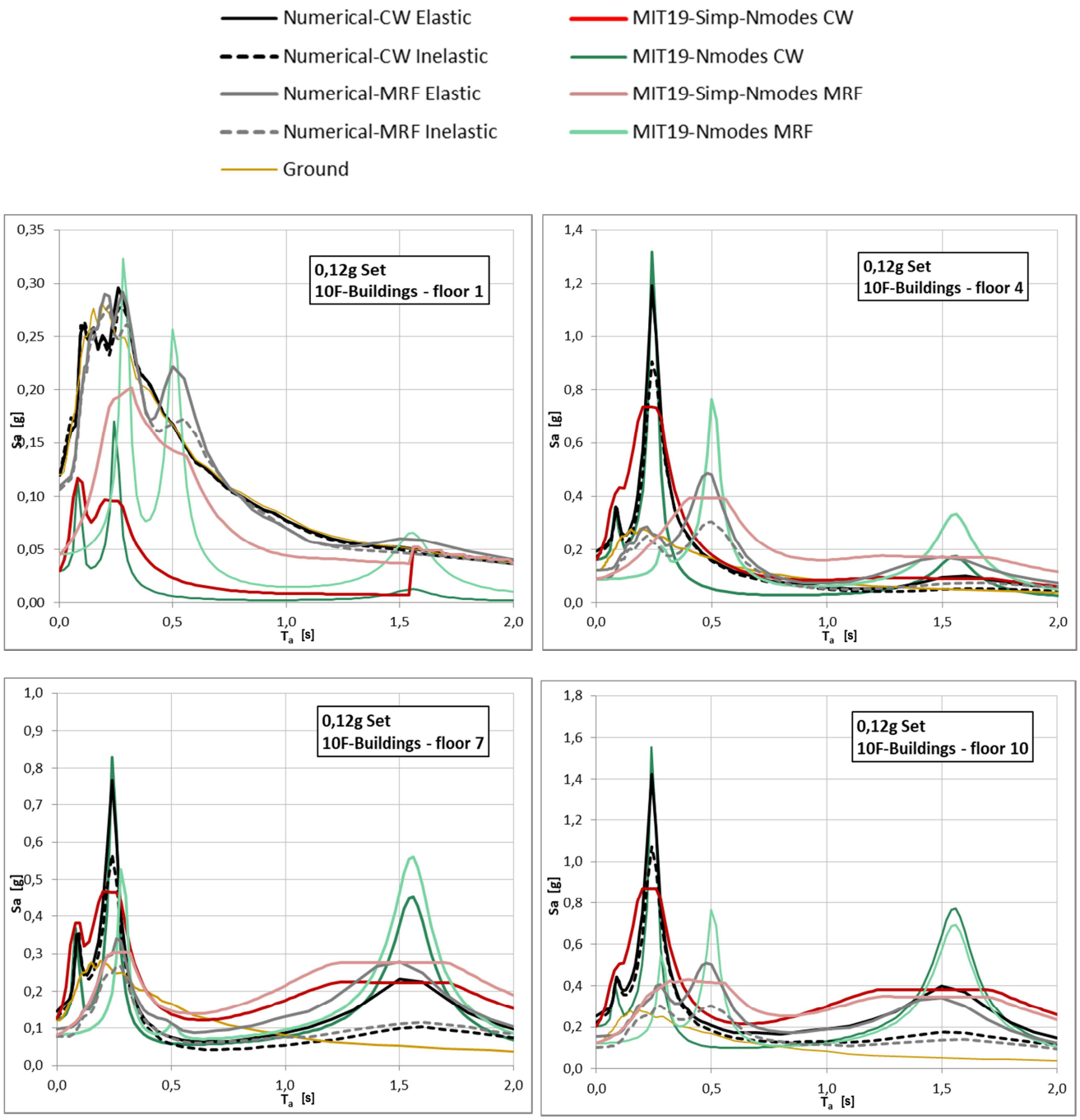

Figure 9: 0.12g Set: 10-story buildings. Numerical floor response spectra obtained by elastic and inelastic analysis compared with those obtained from the modal superposition spectrum-to-spectrum approaches (MIT19-Nmodes and MIT19-Simp-Nmodes).

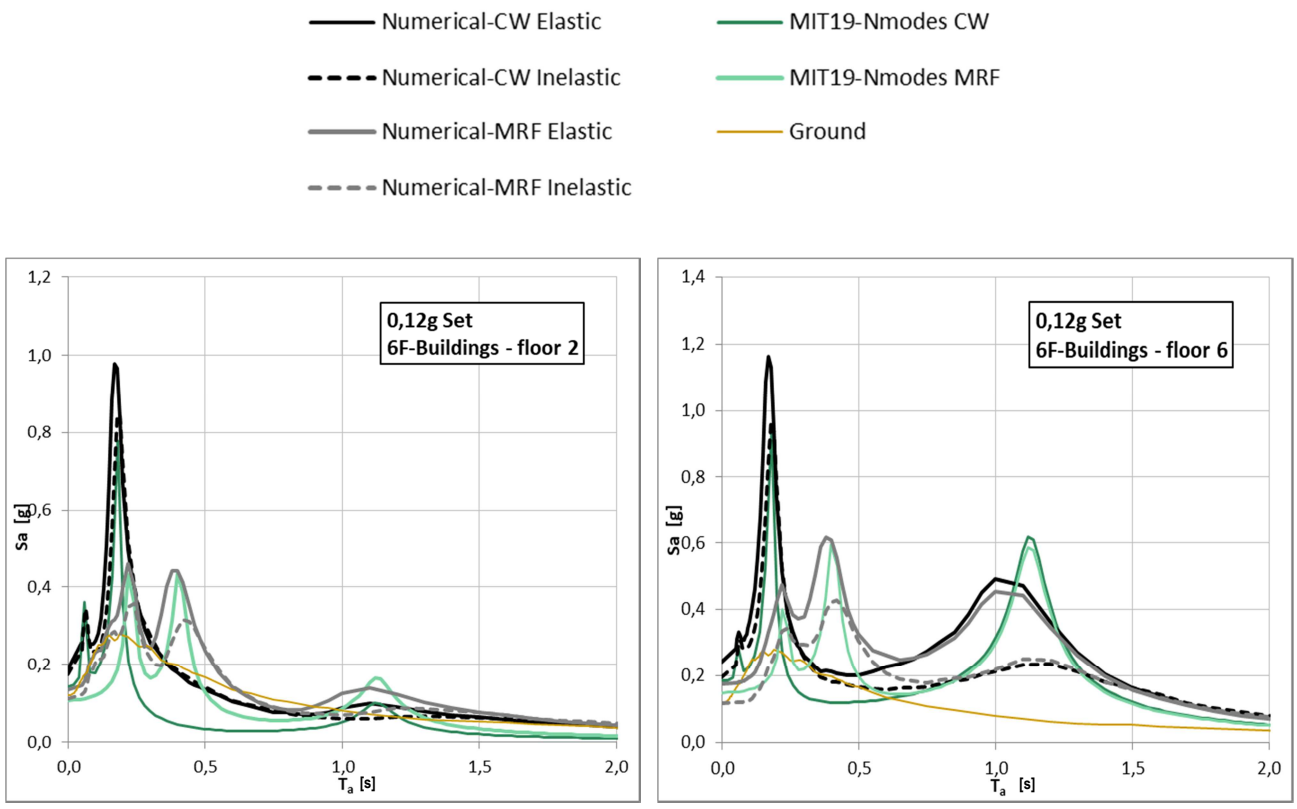

(a) *(b)*

Figure 10: 0.12g Set. Numerical floor response spectra obtained by elastic and inelastic analysis compared with those obtained from MIT19-Nmodes formulation with β = 0.4 for 6-story buildings: (a) 2nd floor; (b) 6th floor.

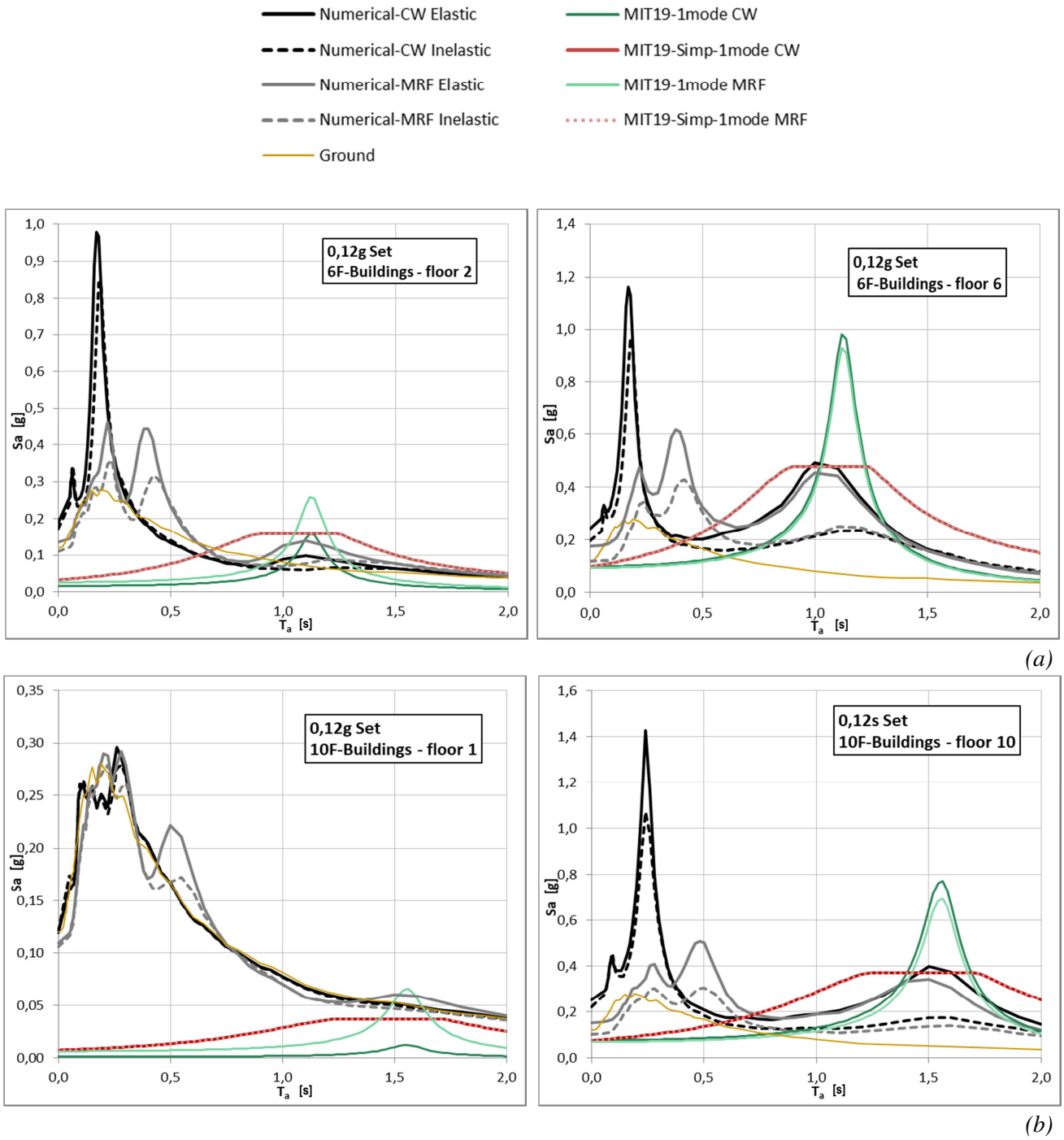

Figure 11: 0.12g Set. Numerical floor response spectra obtained by elastic and inelastic analysis compared with those obtained by MIT19-1mode and MIT19-Simp-1mode: (a) 6-story buildings at 2nd and 6th floors; (b) 10-story buildings at 1st and 10th floors.

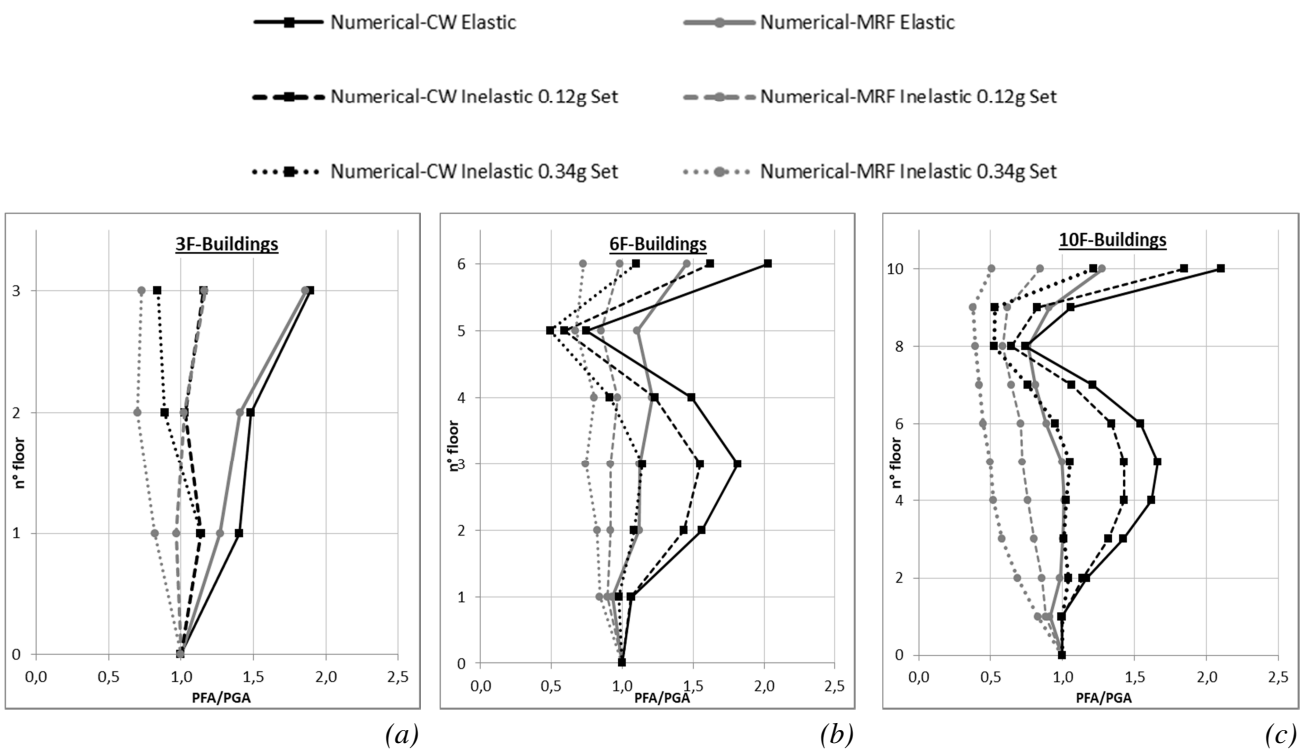

Figure 12: *PFA*/*PGA* profiles versus floor level obtained by elastic and inelastic analysis: (a) 3-story buildings; (b) 6-story buildings; (c) 10-story buildings.

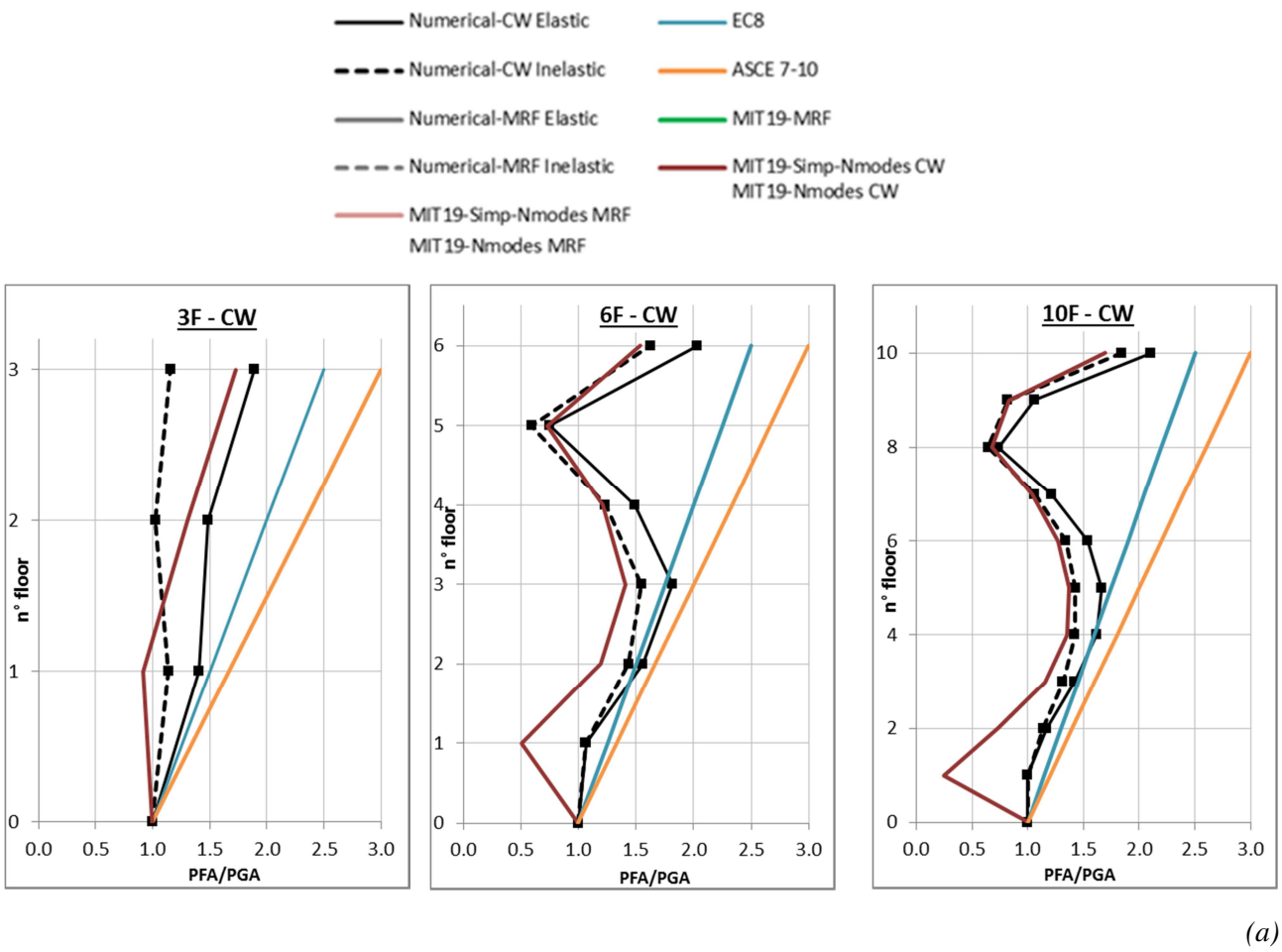

(a)

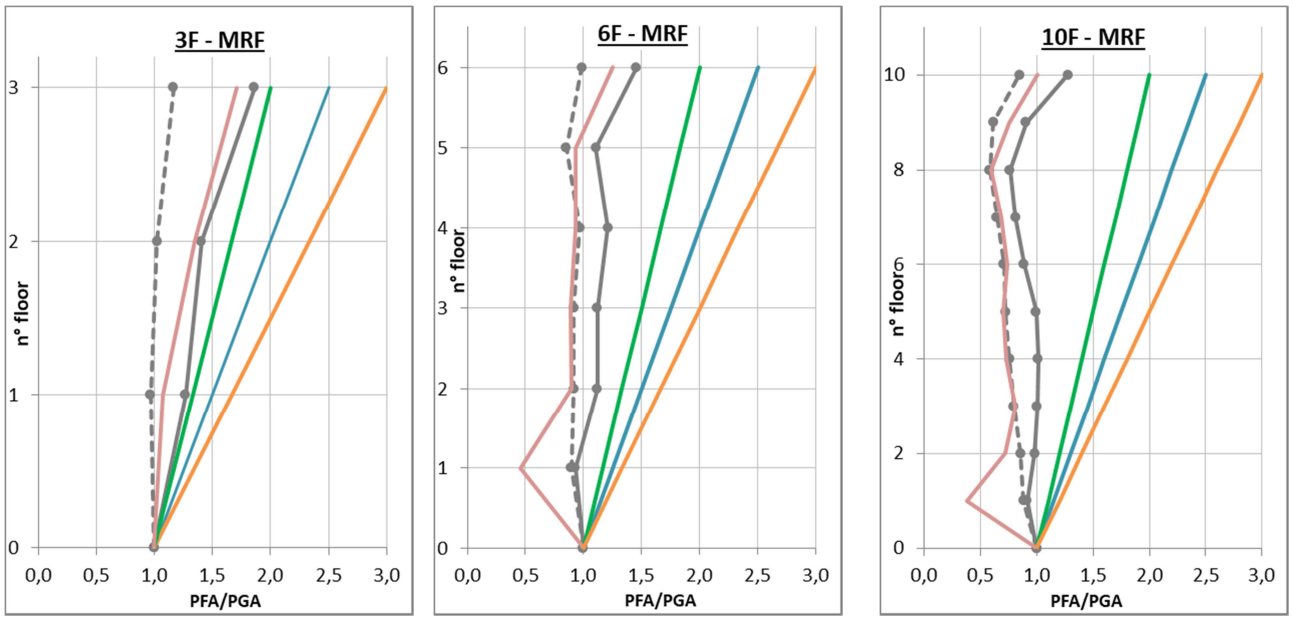

(b)

Figure 13: 0.12g Set. *PFA*/*PGA* profiles versus floor levels obtained by elastic and inelastic analysis compared with the ones obtained by spectrum-to-spectrum approaches: (a) *CW* buildings; (b) *MRF* buildings.

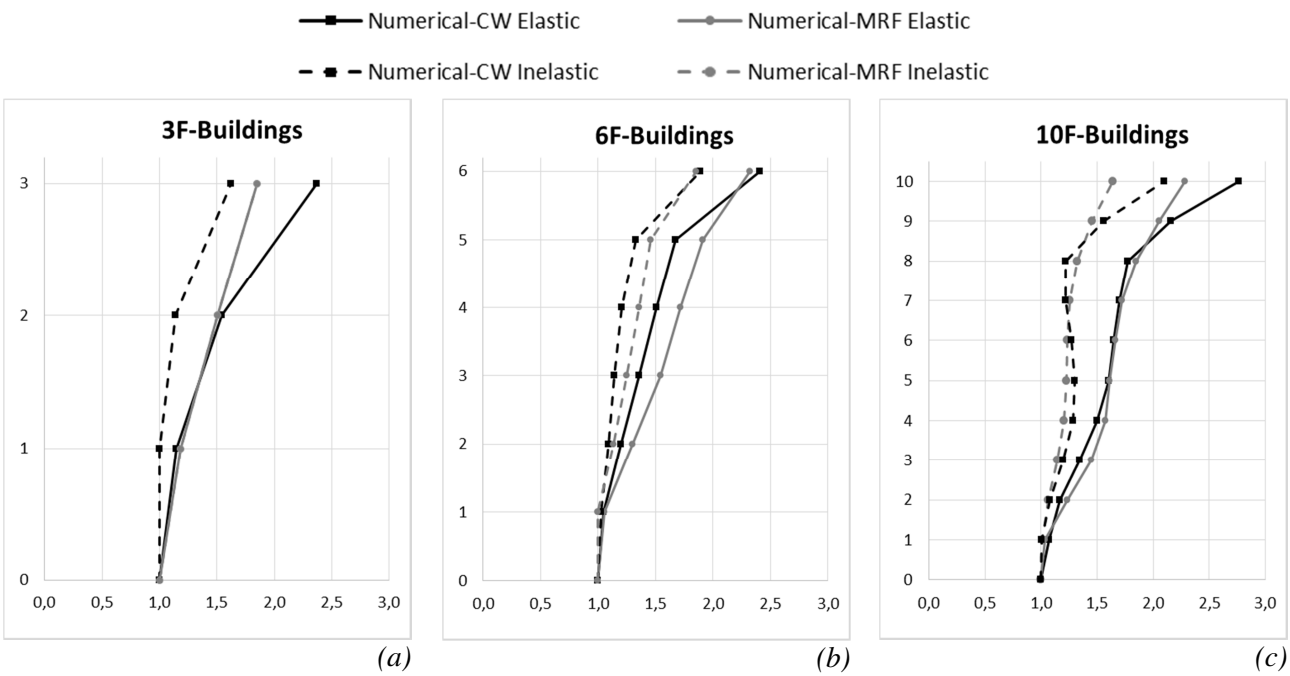

Figure 14: 0.12g Set. *PFV/PGV* profiles: numerical results: (a) 3-story buildings; (b) 6-story buildings; (c) 10-story buildings.

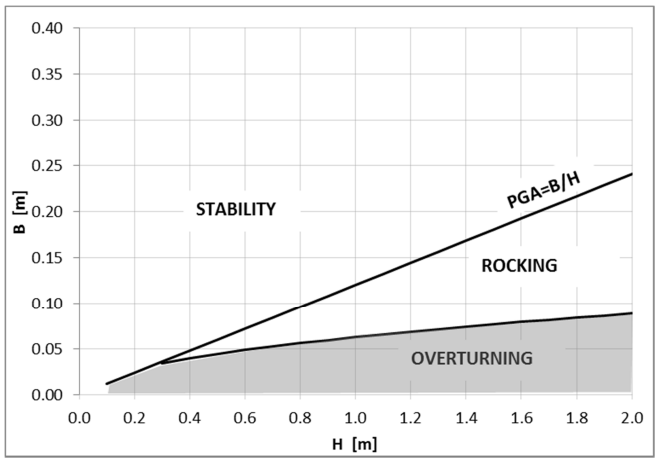

Figure 15 0.12g Set. Overturning stability chart for free standing NS elements at the ground floor

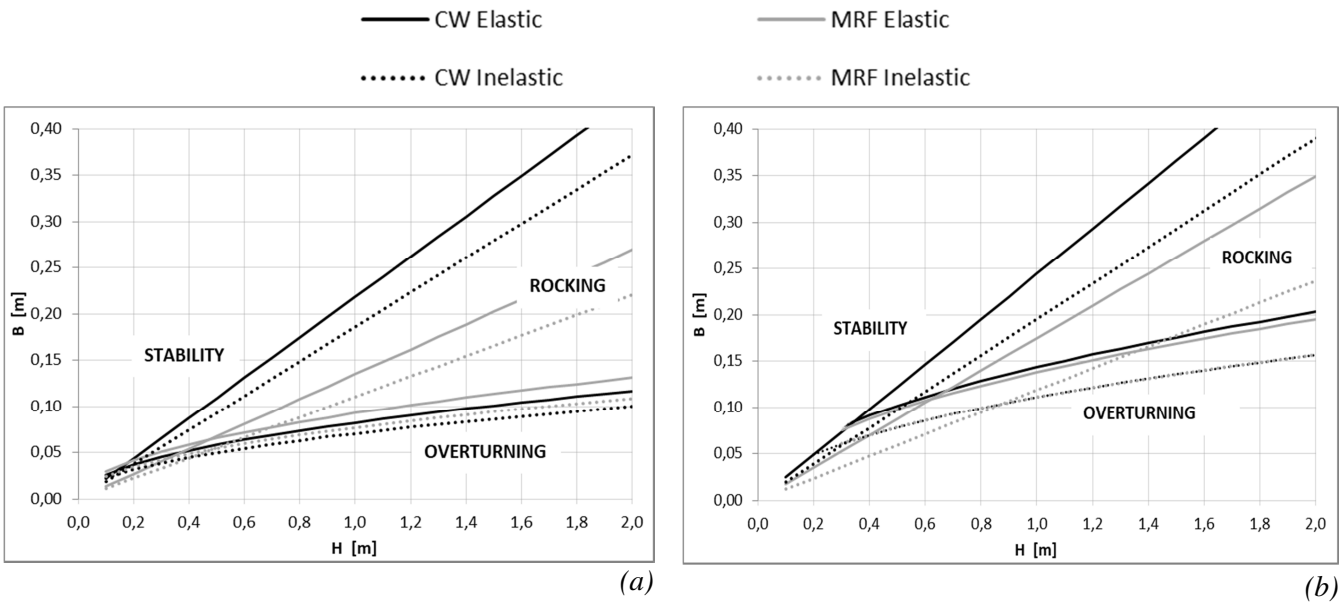

Figure 16 0.12g Set. Overturning stability charts obtained by numerical elastic and inelastic results for 6-story buildings at: (a) 3rd floor level; (b) top level.

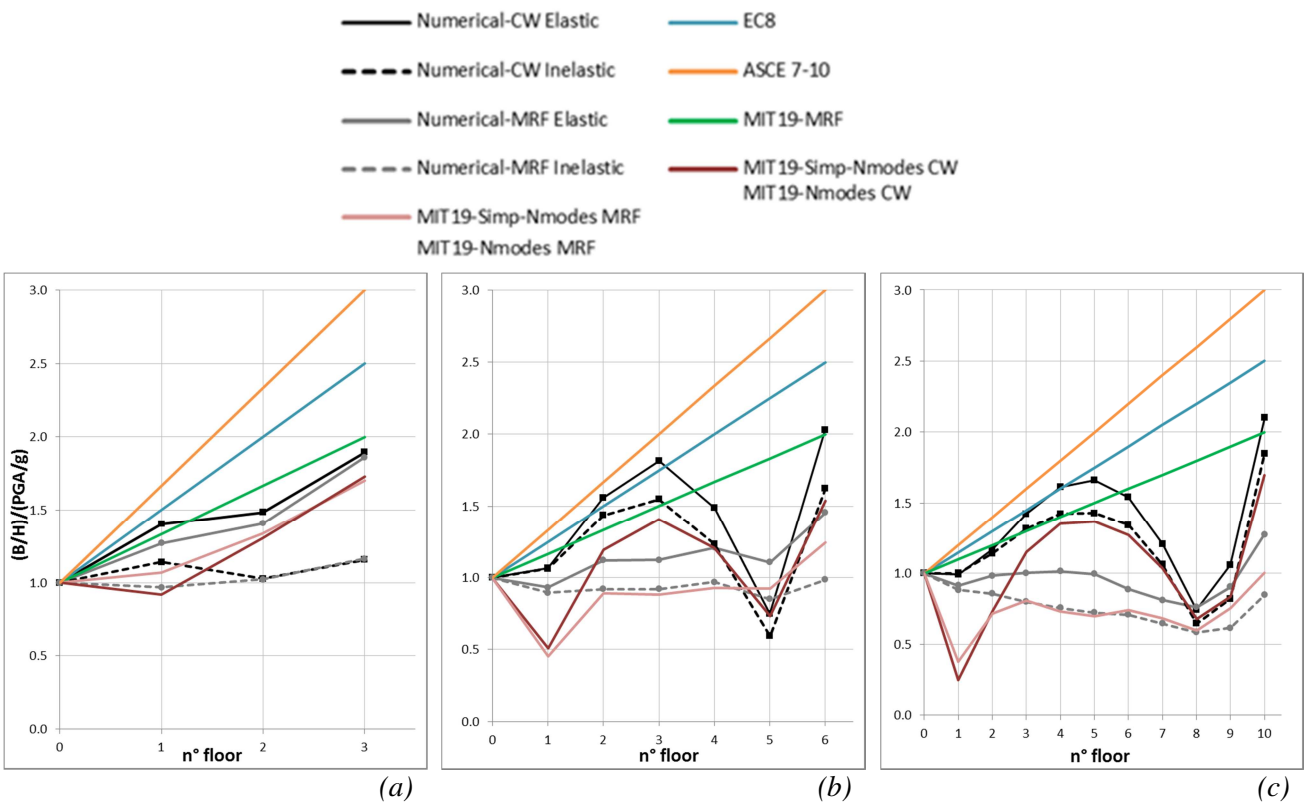

Figure 17: Rocking charts for the case studies at different floor levels: (a) 3-story buildings; (b) 6-story buildings; (c) 10-story buildings.

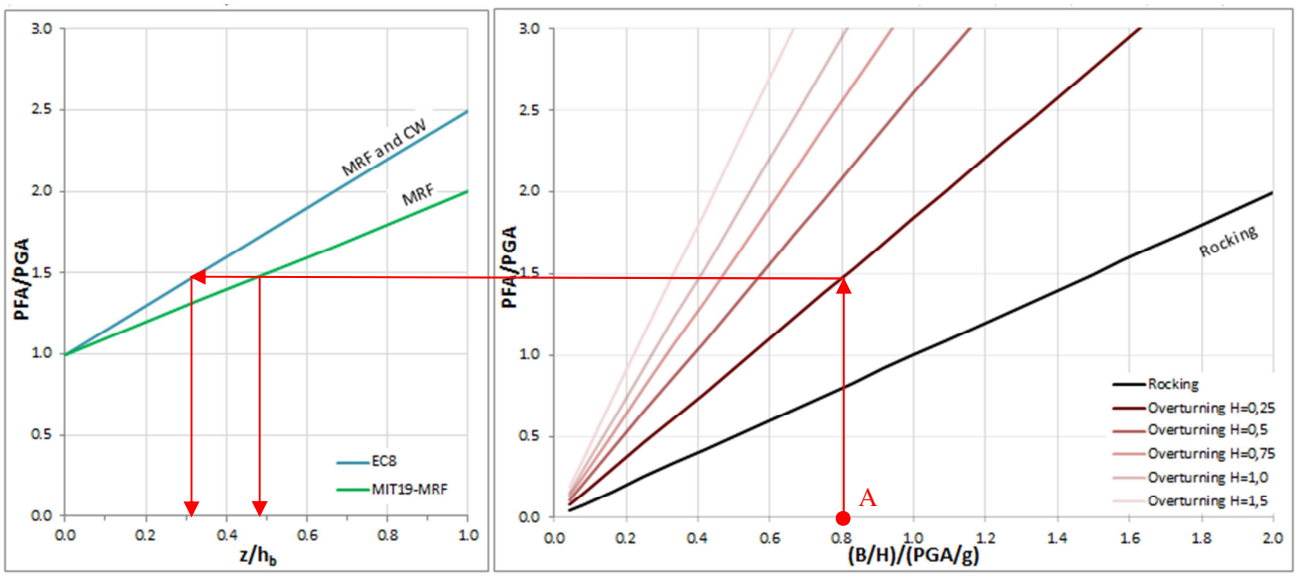

Figure 18: Stability chart of free standing NS elements at different floor levels z/h_b.

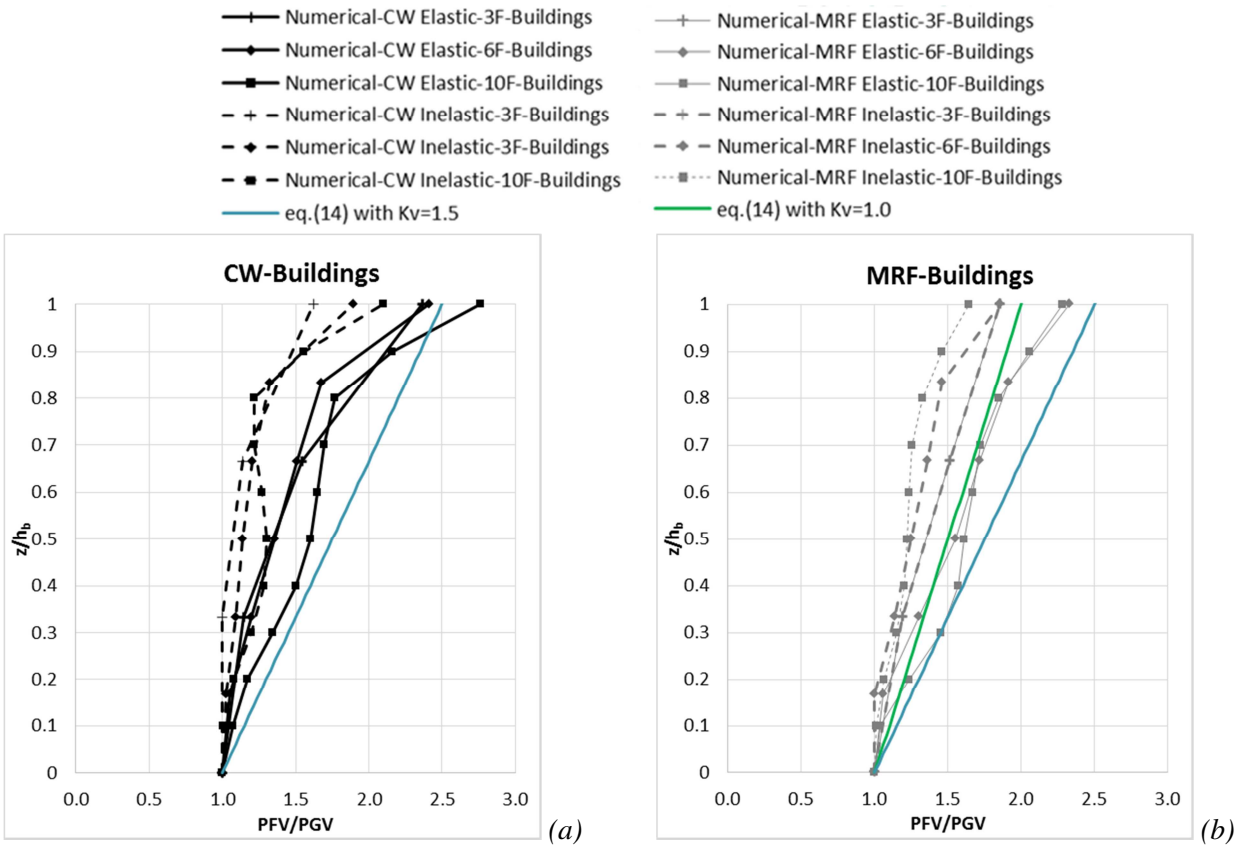

Figure 19: Proposal of a *PFV/PGV* profile compared with those obtained by elastic and inelastic analyses with 0.12g set of time histories: (a) *CW* buildings; (b) *MRF* buildings.

	a	b	a_p
$T_1 < 0,5$ s	0.8	1,4	5,0
0,5 s < T_1 < 1,0 s	0.3	1,2	4,0
$T_1 > 1,0$ s	0.3	1,0	2,5

Table 1 Parameters a, b, a_p of equation (4) (Table C7.2.II Commentary of the Italian Standard)

	3-story building		6-story building		10-story building	
	MRF	*CW*	*MRF*	*CW*	*MRF*	*CW*
T_1 [s] (m_{eff} [%])	0.57 (88.0)	0.57 (72.7)	1.13 (76.5)	1.13 (66.7)	1.56 (80.7)	1.56 (64.5)
T_2 [s] (m_{eff} [%])	0.19 (9.70)	0.09 (21.5)	0.41 (12.1)	0.18 (20.3)	0.51 (11.4)	0.25 (19.8)
T_3 [s] (m_{eff} [%])	0.12 (2.20)	0.03 (5.80)	0.23 (4.90)	0.06 (7.00)	0.29 (3.50)	0.09 (6.80)

Table 2 Periods of vibration and effective modal mass (m_{eff}) for the case study buildings.

No.	Event name	Station	Component [°]	Fault mechanism[§]	M[†]	R[‡] [km]	PGA [g]
1	Northwest Calif-01, 1938	Ferndale City Hall	045	SS	5.50	52.73	0.150
2	Parkfield, 1966	Cholame - Shandon Array #8	050	SS	6.19	12.90	0.248
3	Parkfield, 1966	Temblor pre-1969	205	SS	6.19	15.96	0.357
4	Northern Calif-05, 1967	Ferndale City Hall	224	SS	5.60	27.36	0.253
5	San Fernando, 1971	Castaic - Old Ridge Route	021	R	6.61	19.33	0.320
6	San Fernando, 1971	LA - Hollywood Stor FF	090	R	6.61	22.77	0.225
7	San Fernando, 1971	Lake Hughes #12	021	R	6.61	13.99	0.382
8	San Fernando, 1971	Lake Hughes #4	111	R	6.61	19.45	0.198
9	San Fernando, 1971	Lake Hughes #9	021	R	6.61	17.22	0.170
10	San Fernando, 1971	Palmdale Fire Station	090	R	6.61	24.16	0.112
11	San Fernando, 1971	Pasadena - CIT Athenaeum	000	R	6.61	25.47	0.097
12	San Fernando, 1971	Santa Felita Dam (Outlet)	172	R	6.61	24.69	0.155
13	Friuli_ Italy-01, 1976	Tolmezzo	000	R	6.50	14.97	0.357
14	Friuli_ Italy-02, 1976	Forgaria Cornino	000	R	5.91	14.65	0.261
15	Tabas_ Iran, 1978	Dayhook	090	R	7.35	13.94	0.324
16	Imperial Valley-06, 1979	Calexico Fire Station	225	SS	6.53	10.45	0.277
17	Imperial Valley-06, 1979	Calipatria Fire Station	225	SS	6.53	23.17	0.129
18	Imperial Valley-06, 1979	Cerro Prieto	147	SS	6.53	15.19	0.168
19	Imperial Valley-06, 1979	Compuertas	015	SS	6.53	13.52	0.187
20	Imperial Valley-06, 1979	Delta	262	SS	6.53	22.03	0.236
21	Imperial Valley-06, 1979	El Centro Array #1	140	SS	6.53	19.76	0.141
22	Imperial Valley-06, 1979	El Centro Array #12	140	SS	6.53	17.94	0.145
23	Imperial Valley-06, 1979	El Centro Array #13	140	SS	6.53	21.98	0.118
24	Imperial Valley-06, 1979	Niland Fire Station	090	SS	6.53	35.64	0.110
25	Imperial Valley-06, 1979	Parachute Test Site	225	SS	6.53	12.69	0.113
26	Imperial Valley-06, 1979	Victoria	075	SS	6.53	31.92	0.121
27	Livermore-01, 1980	Del Valle Dam (Toe)	156	SS	5.80	23.92	0.130
28	Mammoth Lakes-01, 1980	Long Valley Dam (UpLAbut)	000	NO	6.06	12.56	0.430
29	Mammoth Lakes-02, 1980	Long Valley Dam (UpLAbut)	000	SS	5.69	14.28	0.193
30	Mammoth Lakes-03, 1980	Convict Creek	090	SS	5.91	2.67	0.233

§ SS: strike-slip; R: reverse; NO: normal oblique.

† Moment magnitude.

‡ Closest distance to fault rupture.

Table 3 0.34g Set: Ultimate Limit State (ULS) ground motions characteristics.

No.	Event name	Station	Component [°]	Fault mechanism§	M†	R‡ [km]	PGA [g]
1	Northwest Calif-01, 1938	Ferndale City Hall	045	SS	5.50	52.73	0.150
2	Northern Calif-01, 1941	Ferndale City Hall	225	SS	6.40	44.52	0.115
3	Borrego, 1942	El Centro Array #9	000	SS	6.50	56.88	0.066
4	Northwest Calif-03, 1951	Ferndale City Hall	224	SS	5.80	53.73	0.108
5	Northern Calif-05, 1967	Ferndale City Hall	224	SS	5.60	27.36	0.253
6	San Fernando, 1971	Gormon - Oso Pump Plant	000	R	6.61	43.95	0.083
7	San Fernando, 1971	Lake Hughes #4	111	R	6.61	19.45	0.198
8	San Fernando, 1971	Lake Hughes #9	021	R	6.61	17.22	0.170
9	San Fernando, 1971	Pasadena - CIT Athenaeum	000	R	6.61	25.47	0.097
10	San Fernando, 1971	Pasadena - Old Seismo Lab	180	R	6.61	21.5	0.095
11	San Fernando, 1971	Pearblossom Pump	000	R	6.61	35.54	0.104
12	San Fernando, 1971	Puddingstone Dam (Abutment)	055	R	6.61	52.64	0.074
13	San Fernando, 1971	Santa Felita Dam (Outlet)	172	R	6.61	24.69	0.155
14	San Fernando, 1971	Whittier Narrows Dam	143	R	6.61	39.45	0.101
15	Santa Barbara, 1978	Santa Barbara Courthouse	132	RO	5.92	12.16	0.101
16	Tabas_ Iran, 1978	Boshrooyeh	000	R	7.35	24.07	0.106
17	Tabas_ Iran, 1978	Ferdows	000	R	7.35	89.76	0.093
18	Coyote Lake, 1979	SJB Overpass_ Bent 3 g.l.	067	SS	5.74	20.44	0.102
19	Coyote Lake, 1979	San J. Bautista, Hwy 101/156	067	SS	5.74	20.44	0.078
20	Coyote Lake, 1979	San J. Bautista, 24 Polk St	213	SS	5.74	19.46	0.112
21	Imperial Valley-06, 1979	Calipatria Fire Station	225	SS	6.53	23.17	0.129
22	Imperial Valley-06, 1979	El Centro Array #1	140	SS	6.53	19.76	0.141
23	Imperial Valley-06, 1979	El Centro Array #13	140	SS	6.53	21.98	0.118
24	Imperial Valley-06, 1979	Niland Fire Station	090	SS	6.53	35.64	0.110
25	Imperial Valley-06, 1979	Parachute Test Site	225	SS	6.53	12.69	0.113
26	Imperial Valley-06, 1979	Victoria	075	SS	6.53	31.92	0.121
27	Imperial Valley-06, 1979	Westmorland Fire Sta	090	SS	6.53	14.75	0.076
28	Livermore-01, 1980	Del Valle Dam (Toe)	156	SS	5.80	23.92	0.130
29	Mammoth Lakes-02, 1980	Long Valley Dam (Up L Abut)	000	SS	5.69	14.28	0.193
30	Mammoth Lakes-03, 1980	Long Valley Dam (Downst)	000	SS	5.91	10.31	0.111

§ SS: strike-slip; R: reverse; NO: normal oblique.
† Moment magnitude.
‡ Closest distance to fault rupture.

Table 4 0.12g Set: Damage Limitation State (DLS) ground motions characteristics

	EC8	**ASCE7-10**	**MIT19-MRFs**
k_a	1.5	2.0	1.0

Table 5 Value of parameter k_a for the different practical approaches